AFRL-RV-PS-
TR-2023-0077

AFRL-RV-PS-
TR-2023-0077

# ADVANCED SATELLITE COMMUNICATIONS RESEARCH

**Hyuck M. Kwon and Richard T. Lahman**

**Wichita State University**
**Department of Electrical Engineering and Computer Science**
**1845 N Fairmount Avenue**
**Wichita, KS 67260-0103**

**30 June 2023**

**Final Report**




**AIR FORCE RESEARCH LABORATORY**
**Space Vehicles Directorate**
**3550 Aberdeen Ave SE**
**AIR FORCE MATERIEL COMMAND**
**KIRTLAND AIR FORCE BASE, NM 87117-5776**

# DTIC COPY

# NOTICE AND SIGNATURE PAGE

Using Government drawings, specifications, or other data included in this document for any purpose other than Government procurement does not in any way obligate the U.S. Government. The fact that the Government formulated or supplied the drawings, specifications, or other data does not license the holder or any other person or corporation; or convey any rights or permission to manufacture, use, or sell any patented invention that may relate to them.

This report is the result of contracted fundamental research which is exempt from public affairs security and policy review in accordance with AFI 61-201, paragraph 2.3.5.1. This report is available to the general public, including foreign nationals. Copies may be obtained from the Defense Technical Information Center (DTIC) (http://www.dtic.mil).

AFRL-RV-PS-TR-2023-0077 HAS BEEN REVIEWED AND IS APPROVED FOR PUBLICATION IN ACCORDANCE WITH ASSIGNED DISTRIBUTION STATEMENT.

| | |
|---|---|
| //SIGNED// | //SIGNED// |
| Dr. Steven A. Lane<br>Program Manager, AFRL/RVB | For: Mark E. Roverse, Chief<br>AFRL Geospace Technologies Division |

This report is published in the interest of scientific and technical information exchange, and its publication does not constitute the Government's approval or disapproval of its ideas or findings.

# REPORT DOCUMENTATION PAGE

*Form Approved*
*OMB No. 0704-0188*



| **1. REPORT DATE** *(DD-MM-YYYY)* | **2. REPORT TYPE** | **3. DATES COVERED** *(From - To)* |
|---|---|---|
| 30-06-23 | Final Report | 02 Feb 2018 – 31 Mar 2023 |

**4. TITLE AND SUBTITLE**
Advanced Satellite Communications Research

**5a. CONTRACT NUMBER**
FA9453-21-2-0011

**5b. GRANT NUMBER**

**5c. PROGRAM ELEMENT NUMBER**
63401F

**6. AUTHOR(S)**
Hyuck M. Kwon and Richard T. Lahman

**5d. PROJECT NUMBER**
3682

**5e. TASK NUMBER**
EF134013

**5f. WORK UNIT NUMBER**
V1M6

**7. PERFORMING ORGANIZATION NAME(S) AND ADDRESS(ES)**
Wichita State University
Department of Electrical Engineering and Computer Science
1845 N Fairmount Avenue
Wichita, KS 67260-0103

**8. PERFORMING ORGANIZATION REPORT NUMBER**

**9. SPONSORING / MONITORING AGENCY NAME(S) AND ADDRESS(ES)**
Air Force Research Laboratory
Space Vehicles Directorate
3550 Aberdeen Avenue SE
Kirtland AFB, NM 87117-5776

**10. SPONSOR/MONITOR'S ACRONYM(S)**
AFRL/RVBYC

**11. SPONSOR/MONITOR'S REPORT NUMBER(S)**
AFRL-RV-PS-TR-2023-0077

**12. DISTRIBUTION / AVAILABILITY STATEMENT**
Approved for public release; distribution is unlimited (AFRL-2023-3726 dtd 14 Jul 2023).

**13. SUPPLEMENTARY NOTES**

**14. ABSTRACT**

The Digital Video Broadcasting - Second Generation (DVB-S2) satellite communication system is considered under (1) a memoryless flat (i.e., single multipath) Rayleigh fading, (2) a frequency selective (i.e., multiple multipath) Rayleigh fading, (3) a flat Rician fading, and (4) a frequency-selective Rician fading channel. The bit error rate (BER) of the DVB-S2 under these fading channels could not reach 10-5 with practical symbol-energy-to-noise ratio except a flat Rician fading multipath channel of a high Rician factor K. The bandwidth efficiency of the W/V-band is computed at 10-2 BER. Orthogonal frequency division multiplexing (OFDM) was used under frequency-selective fading before the DVB-S2 decoding. It was observed that the polar code in the fifth generation (5G) system of simpler complexity performed better than DVB-S2 low-density parity-check (LDPC) forward error correction code (FEC) under both flat and frequency-selective fading. Since the 5G network being employed may not be trustable, bit streams were encrypted before a FEC channel encoder and decrypted after a FEC channel decoder as a double layer encryption with simple complexity but no performance degradation.

**15. SUBJECT TERMS**
space communication; W/V-band, waveform simulations, code modulation, bit error rate

| **16. SECURITY CLASSIFICATION OF:** | | | **17. LIMITATION OF ABSTRACT** | **18. NUMBER OF PAGES** | **19a. NAME OF RESPONSIBLE PERSON** |
|---|---|---|---|---|---|
| **a. REPORT** | **b. ABSTRACT** | **c. THIS PAGE** | | | Dr. Steven A. Lane |
| Unclassified | Unclassified | Unclassified | Unlimited | 80 | **19b. TELEPHONE NUMBER** *(include area code),* |

This page is intentionally left blank.

# TABLE OF CONTENTS


**Section** **Page**

LIST OF FIGURES ..... ii
LIST OF TABLES ..... iv
1 SUMMARY ..... 1
2 INTRODUCTION ..... 2
2.1 Motivation ..... 2
2.2 Objective ..... 2
2.3 Background ..... 2
2.4 Overview ..... 3
3 METHODS, ASSUMPTIONS AND PROCEDURES ..... 4
3.1 Additive White Gaussian Noise Model ..... 4
3.2 Flat Rayleigh Fading Channel Model ..... 6
3.3 Frequency Selective Rayleigh Fading Channel Model ..... 17
3.4 Flat Rician Fading Channel Model ..... 22
3.5 Frequency Selective Rician Fading Channel Model ..... 28
3.6 5G Polar FEC and Flat Rayleigh Fading ..... 35
3.7 Double Layer Encryption ..... 41
4 RESULTS AND DISCUSSION ..... 44
4.1 5G Polar FEC and Flat Rayleigh Fading ..... 44
4.2 Double Layer Encryption ..... 46
5 CONCLUSIONS ..... 51
REFERENCES ..... 52
APPENDIX 1 MATLAB Source Code for Flat Rayleigh Fading ..... 54
APPENDIX 2 MATLAB Source Code for Frequency Selective Rayleigh Fading ..... 55
APPENDIX 3 MATLAB Source Code for Flat Rician Fading ..... 57
APPENDIX 4 MATLAB Source Code for Frequency Selective Rician Fading ..... 58
APPENDIX 5 MATLAB Source Code for 5G Polar FEC and Flat Rayleigh Fading ..... 60
APPENDIX 6 MATLAB Source Code for Double Layer Encryption ..... 63
LIST OF SYMBOLS, ABBREVIATIONS AND ACRONYMS ..... 68

## LIST OF FIGURES

**Figure** **Page**


Figure 1. Block Diagram of Digital Video Broadcasting - Second Generation (DVB-S2), Including LDPC Coding ..... 4

Figure 2. BER vs $E_s/N_0$ for DVB-S2 Under AWGN with QPSK and Different LDPC Code Rates ..... 6

Figure 3. WTLE Test Range Setup for Measuring Attenuation Statistics for Channel Modeling . 7

Figure 4. Received Power Data Obtained in 2019 from WTLE ..... 7

Figure 5. BER vs $E_s/N_0$ for DVB-S2 Under Flat Rayleigh Fading with QPSK and Different LDPC Code Rates ..... 8

Figure 6. BER vs $Es/N_0$ for DVB-S2 Under Flat Rayleigh Fading with 8PSK and Different LDPC Code Rates ..... 9

Figure 7. BER vs $E_s/N_0$ for DVB-S2 Under Flat Rayleigh Fading with 16PSK and Different LDPC Code Rates ..... 9

Figure 8. BER vs $E_s/N_0$ for DVB-S2 Under Flat Rayleigh Fading with 32PSK and Different LDPC Code Rates ..... 10

Figure 9. CDF $F_X(x)$ of Attenuation Random Variable $X$ ..... 13

Figure 10. OFDM Channel Frequency Response ..... 18

Figure 11. DVB-S2 QPSK Two Multipath Rayleigh Fading With OFDM ..... 19

Figure 12. DVB-S2 8PSK Two Multipath Rayleigh Fading with OFDM ..... 20

Figure 13. DVB-S2 16APSK Two Multipath Rayleigh Fading With OFDM ..... 20

Figure 14. DVB-S2 32APSK Two Multipath Rayleigh Fading with OFDM ..... 21

Figure 15. BER vs $E_s/N_0$ for DVB-S2 Under Flat Rician Fading with QPSK and Different LDPC Code Rates ..... 23

Figure 16. BER vs $E_s/N_0$ for DVB-S2 Under Flat Rician Fading with 8PSK and Different LDPC Code Rates ..... 24

Figure 17. BER vs $E_s/N_0$ for DVB-S2 Under Flat Rician Fading with 16APSK and Different LDPC Code Rates ..... 24

Figure 18. BER vs $E_s/N_0$ for DVB-S2 Under Flat Rician Fading with 32APSK and Different LDPC Code Rates ..... 25

Figure 19. DVB-S2 QPSK Two Multipath Rician Fading with OFDM ..... 31

Figure 20. DVB-S2 8PSK Two Multipath Rician Fading with OFDM ..... 32

Figure 21. DVB-S2 16APSK Two Multipath Rician Fading with OFDM ..... 32

Figure 22. DVB-S2 32APSK Two Multipath Rician Fading with OFDM ..... 33

Figure 23. Binary Tree Representation for Level 2 Output Bits ..... 36

Figure 24. Binary Tree Representation for Level 4 Output Bits ..... 37

## LIST OF FIGURES (continued)

**Figure** **Page**

Figure 25. Assigned Message Bits and Frozen Bits ..... 38
Figure 26. Two Received Bits $r_1$ and $r_2$ That are Beliefs for $x_1$ and $x_2$ ..... 39
Figure 27. Basic Building Block of How the Message is Passed on the Tree ..... 39
Figure 28. A General Block Diagram of the 5G Transmitter and Receiver ..... 40
Figure 29. A Flow Diagram Between Alice, Bob, and Eve ..... 42
Figure 30. BER versus $E_s/N_0$ For Both Polar Code and LDPC Code Under AWGN Channel ..... 44
Figure 31. BER versus $E_s/N_0$ For Both Polar Code and LDPC Code Under Flat Rayleigh Fading Channel ..... 45
Figure 32. BER versus $E_s/N_0$ For Both Polar Code and LDPC Code Under Frequency Selective Rayleigh Fading Channel ..... 46
Figure 33. BER Under AWGN Channel With and Without Encryption ..... 47
Figure 34. BER versus SNR Under a Single Multipath Rayleigh Fading ..... 48
Figure 35. BER versus SNR Under Two Multipath Rayleigh Fading ..... 49
Figure 36. BER versus SNR Under Two Multipath Rician Fading with Rician Factor $K$= 12 dB ..... 50

## LIST OF TABLES

**Table** **Page**

Table 1. Required $E_s/N_0$ at $P_b = 10^{-2}$ and Bandwidth Efficiency Under Flat Rayleigh Fading and Link Margin of 25.871 dB ..... 12

Table 2. BWE Results Under Flat Rayleigh Fading with BW=5 GHz ..... 16

Table 3. BWE Results Under AWGN with BW=5 GHz ..... 16

Table 4. BWE Results Under Two Multipath Rayleigh Fading Channel and OFDM with BW=5 GHz ..... 22

Table 5. Required $E_s/N_0$ at $P_b = 10^{-2}$ and BWE Under Two Multipath Rayleigh Fading with OFDM and Link Margin of 16.36 dB ..... 22

Table 6. Required $E_s/N_0$ at $P_b = 10^{-5}$ and BWE Under Flat Rician Fading and Link Margin of 21.401 dB ..... 26

Table 7. BWE Results Under Flat Rician Fading with BW = 5 GHz ..... 28

Table 8. BWE Results Under AWGN with BW = 5 GHz ..... 28

Table 9. BWE Results Under Two Multipath Rician Fading Channel of Rician Factor $K$ = 12 dB with OFDM and BW=5 GHz ..... 34

Table 10. Required $E_s/N_0$ at $P_b = 10^{-2}$ and BWE Under Two Multipath Rician Fading with OFDM and Link Margin of 8.828 dB ..... 35

Table 11. List of Modulo-2 Additions ..... 36

## ACKNOWLEDGMENTS

This material is based on research sponsored by Air Force Research Laboratory under agreement number FA9453-21-2-0011. The U.S. Government is authorized to reproduce and distribute reprints for Governmental purposes notwithstanding any copyright notation thereon.

## DISCLAIMER

The views and conclusions contained herein are those of the authors and should not be interpreted as necessarily representing the official policies or endorsements, either expressed or implied, of Air Force Research Laboratory or the U.S. Government.

This page is intentionally left blank.

# 1 SUMMARY

During this contract, Advanced Satellite Communications Research, the impact on wireless communication system performance was investigated for five channel conditions, which included (1) additive white Gaussian noise, (2) flat Raleigh fading, (3) frequency selective Raleigh fading, (4) flat Rician fading, and (5) frequency selective Rician fading. Models and simulations implemented the DVB-S2 communications protocol, which used various modulation methods, forward error correction, and interleaving. Simulations used measured attenuation data provided by the Air Force Research Laboratory at 72 GHz from a 26.3 km propagation test range. Models and simulations were also developed and presented to investigate and compare 5G network technology, which included orthogonal frequency division multiplexing and polar error correction coding. Finally, an analysis of the effects of double layer encryption the wireless communication system performance was investigated.

# 2 INTRODUCTION

## 2.1 Motivation

New algorithm strategies and diverse communication techniques are constantly emerging in the telecommunications realm that consumers, commercial, government, and military demand in order to push the boundaries of data throughput to receive information as quickly as possible. Currently, the Ku/Ka satellite band (20–30 GHz) becomes congested during peak service. There has been a strong demand for a wider bandwidth and higher data rate in both cellular and satellite communication service. As the carrier frequency increases, a wider bandwidth can be made available, and a higher data rate can be obtained with beamforming or precoding. Particularly, the V band (50–75 GHz) and W band (75–110 GHz) offer unprecedented broadband capabilities and extremely large contiguous allocations of bandwidth. This is the reason NASA and AFRL have been investigating these bands for civilian and military use.

At W/V-band, the wavelength is on the order of 3 to 4 millimeters. Thus, receivers can be implemented via very small devices. Further, a W/V-band system can have a very narrow beam-angle-spread, which can significantly reduce the interference among beams and recover propagation loss.

When a new wireless terrestrial or satellite communication system is planned, the channel path attenuation data is typically collected first by transmitting a carrier frequency signal without modulation under a line-of-sight (LOS) and an Additive White Gaussian Noise (AWGN) environment. Since the transmit power, $P_T$, and the distance, $d_{TR}$, between a transmitter (TX) and a receiver (RX) are known, the free space path loss, $P_{path} = (\lambda/4\pi d_{TR})^2$, can be precalculated for a given wavelength $\lambda = c/f_c$, i.e., a given carrier frequency $f_c$ where $c$ is the speed of the light. Hence, the channel attenuation, $P_{attn}$ due to the channel medium can be obtained as $P_{attn} = P_T - P_R - P_{path}$ by measuring the received power $P_R$ at the RX for a given transmitted power $P_T$. The difference, $P_{attn}$, will be called the channel attenuation in this report. These channel attenuation data can be obtained more economically than by sending a modulated signal. Data enables an RF communication system engineer to determine the appropriate transmit power, antenna type, antenna size, modulation type, forward error correction coding type, code rate, and data rate.

## 2.2 Objective

The technical objective of this project was to investigate bandwidth efficiency of wireless communication waveforms under Rayleigh and Rician fading environments, in addition to additive white Gaussian noise, for satellite communication links. Initial research, simulations, and analyses are presented in this report, but the entire scope of work was not completed due to limitation of funds and pre-mature termination of the program.

## 2.3 Background

A LOS and AWGN environment was used for practical channel attenuation measurements in 2019 for a W/V-band channel [1, 2]. From this, the principal investigator (PI) and graduate research

assistants (GRAs) generated a technical report and published the bandwidth efficiency of the W/V-band channel under the AWGN channel environment [3, 4]. However, no channel fading was included in the channel attenuation measurement data. Hence, the channel attenuation data represents the attenuation due to the path loss and weather conditions only.

Channel fading degrades the communication link quality. Fading is mainly caused by the addition of multipath received signals where each path signal phase is randomly shifted from that of the ideally received signal under no fading, and each multipath signal amplitude is distorted. This fading is caused by scattering, reflection, and refraction at the surface of objects in the channel medium. Hence, the phase of the summed received signal at a given time is typically random. Therefore, the receiver must be able to estimate the fading coefficient before coherent demodulation.

For fading effect analysis, the average power of a fading coefficient is typically assumed to be 1, which means no power degradation. This fading is called a small-scale fast fading while the measured path loss attenuation is called a large-scale slow fading. In practice, only channel attenuation data (caused by the path loss and weather conditions) are available and are relatively slowly varying while the small-scale fading coefficient changes fast. In this project, the small-scale fading was included in the bandwidth efficiency analysis.

### 2.4 Overview

In this work, the same bandwidth efficiency (BWE) conversion method described in reference [3] and [4] were used to model the estimated BWE of a W/V-band channel under Rayleigh and Rician fading. Both flat fading and frequency selective fading were considered for both types of fading (i.e., Rayleigh and Rican). Measured data from the W/V-band Terrestrial Link Experiment were used to model the communications channel. Simulations were conducted using adaptive code modulation (ACM) methods included in the Digital Video Broadcasting – Second Generation (DVB-S2) communications protocol. Simulations and analysis was accomplished using Matlab tools. The DVB-S2 satellite link protocol has been in existence since 2014 and includes 28 possible combinations of forward error correction (FEC) coding and modulations depending on the channel conditions [5, 6, 7].

Further, polar error-correction code, which has been used in the fifth generation (5G) terrestrial communication system, was investigated [8, 9, 10, 11]. The bit error rate (BER) of the polar code under AWGN and Rayleigh fading environment was compared with that of the low-density parity check (LDPC), which has been used in the DVB-S2 satellite communications system.

Finally, modeling and simulations were conducted for a simple double layer encryption method to protect against eavesdropping.

# 3 METHODS, ASSUMPTIONS AND PROCEDURES

## 3.1 Additive White Gaussian Noise Model

A block diagram for a communications channel is shown in Figure 1. This model was presented in prior work [4]. It illustrates the implementation of the DVB-S2 communications protocol. The DVB-S2 communication link begins by generating a sequence of bits to form a data set to build a "packet". Packets of data are assembled into frames (block "BBFrame Buffering"). Then, the frame is encoding by using the Bose-Chaudhuri-Hocquenghem (BCH) and Low-Density Parity Check (LDPC) encoding algorithms. [6], [7]. Once encoded, the data stream enters the interleaver block where it is converted (shuffled) into a "memoryless" bit stream. Error correction and interleaving are commonly applied in wireless communication systems to mitigate bit errors resulting from scintillation and fading. After encoding and interleaving, the data stream is modulated according to the user's and channel parameters before being transmitted through the physical medium (e.g., free space). Modulation determines the bits of transmitted data per second, or as in our case, the symbols transmitted per second. DVB-S2 employs an adaptive coding modulation (ACM) scheme so that the modulation can be supported by the existing channel conditions (i.e., the ratio of the energy per symbol to the channel noise power, $E_S/N_0$). Modulation schemes include quadrature phase shift keying (QPSK), 8 phase shift keying (8PSK), 16 amplitude phase shift keying (16APSK), and 32 amplitude phase shift keying (32APSK). Error correction coding can vary the ratio of the number of check bits to data bits. The various ratios used for forward error correction (FEC) are denoted as {1/4, 1/2, 3/5, 2/3, 3/4, 4/5, 5/6, and 9/10}. The code modulation scheme is adjusted (i.e., adapted) to achieve required performance (e.g., bit error rate or packet error rate). The process is reversed once the data stream is received. DVB-S2 employs a return channel (i.e., feedback mechanism) to provide channel information back to the transmitter so that the modulation scheme can be adapted as appropriate. Additional details of the DVB-S2 algorithm can be found in references [5, 12]

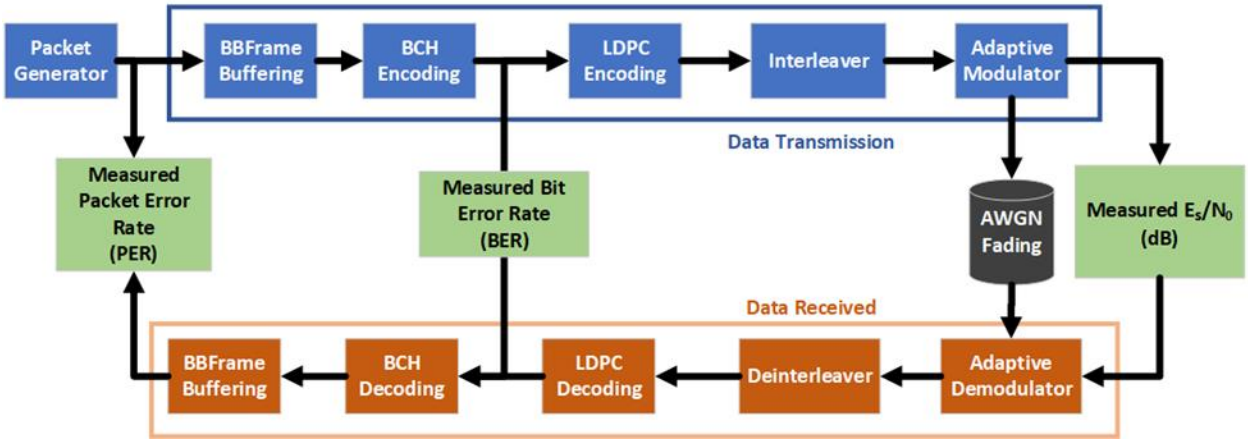


**Figure 1. Block Diagram of Digital Video Broadcasting - Second Generation (DVB-S2), Including LDPC Coding**

For Quadrature Phase Shift Keying (QPSK) modulation, the modulation order is $M = 4$. Thus, there are 2 bits of information transmitted in each "symbol" (recall that the number of bits per symbol is given by $\log_2(M)$ [13]). This is the lowest modulation order for DVB-S2. If the modulation order increases, then the required ratio of energy per symbol to channel noise power ($E_s/N_0$) increases. More signal power is required to maintain the target quality of service (i.e., packet error rate). If the channel noise is low, then it is reasonable that the modulation order be increased to maximize the number of symbols per second (i.e., data rate). A higher rate of symbols per second increase the bandwidth efficiency of the communications channel. Thus, a high-order modulation scheme such as 32APSK provides better bandwidth efficiency than a lower order modulation scheme such as QPSK. Ultimately, the $E_s/N_0$ determines the modulation scheme that can be supported by the physical channel.

When forward error correction is applied, the ratio of the uncoded bit rate, $k$, to the coded bit rate, $n$, is called the code rate, $R_c = k/n$ (i.e., 1/4, 1/2, 2/3, …}. Therefore, if the channel is "bad" (i.e., low $E_s/N_0$) then the code rate must adjust to send more correction / redundant bits (i.e., go from 2/3 to 1/4) to maintain the target performance (i.e., probability of bit error, $P_b$). Since more of the transmitted data are correction / redundant bits, the channel efficiency suffers. Forward error correction code also referred to as ($n$, $k$) codes (i.e., (4,1), (2,1), (3,2)).

Figure 1 indicates an average white Gaussian noise channel (AWGN). Although realistic for many situations, additive Gaussian noise channel models do not accurately represent many transmission phenomena. Other important sources of degradation in many digital data systems are (1) bandlimiting of the signal by the channel, (2) non-Gaussian noise such as impulse noise due to lightning or switches, (3) radio frequency interference due to other transmitters, and (4) multiple transmission paths, termed multipath, due to stratification in the transmission medium or objects that reflect or scatter the propagating signal [14].

We can assume that there are several delayed multipath components at the receiver with random amplitudes and phases. Applying the central-limit theorem, it follows that the in-phase and quadrature components of the received signal are Gaussian, the sum total of which we refer to as the diffuse component. In some cases, there may be one dominant component due to a direct line-of-sight from the transmitter to the receiver, which we refer to as the specular component. It can be shown that the envelope of the received signal obeys a Ricean probability density function, given by

$$f_R(r) = \frac{r}{\sigma^2} \exp\left(-\frac{(r^2+A^2)}{2\sigma^2}\right) I_0\left(\frac{rA}{\sigma^2}\right), \quad r \geq 0 \tag{1}$$

where $A$ is the amplitude of the specular component, $\sigma^2$ is the variance of each quadrature diffuse component, and $I_0(u)$ is the modified Bessel function of the first kind and order zero. Note that if A = 0, then the Ricean probability density function reduces to a Rayleigh probability density function [15].

Implicit in this channel model as just discussed in that the envelope of the received signal varies slowly compared with the bit interval. This is known as a *slowly fading* channel. If the envelope

(and phase) of the received signal envelope and/or phase varies nonnegligibly over the bit interval, the channel is said to be *fast fading*. This is a more difficult case to analyze than the slowly fading case. A common model for the envelope of the received signal in the slowly fading case is a Rayleigh random variable, which is also the simplest case to analyze. Somewhat more general, but more difficult to analyze, is to model the envelope of the received signal as a Ricean random variable [15].

For reference, Figure 2 shows the BER versus $E_s/N_0$ in dB for the DVB-S2 under the AWGN with QPSK and different LDPC code rates. Observe that the QPSK with the highest LDPC code rate 9/10 can achieve $10^{-5}$ BER at $E_s/N_0$ = 6.3 dB. Hence, this $E_s/N_0$ = 6.3 dB will be assumed to be the normal operating signal-to-noise ratio when the available ACM modes in the DVB-S2 are only QPSK of different code rates. If there is further channel attenuation degradation, then a next possible lower ACM mode must be found.

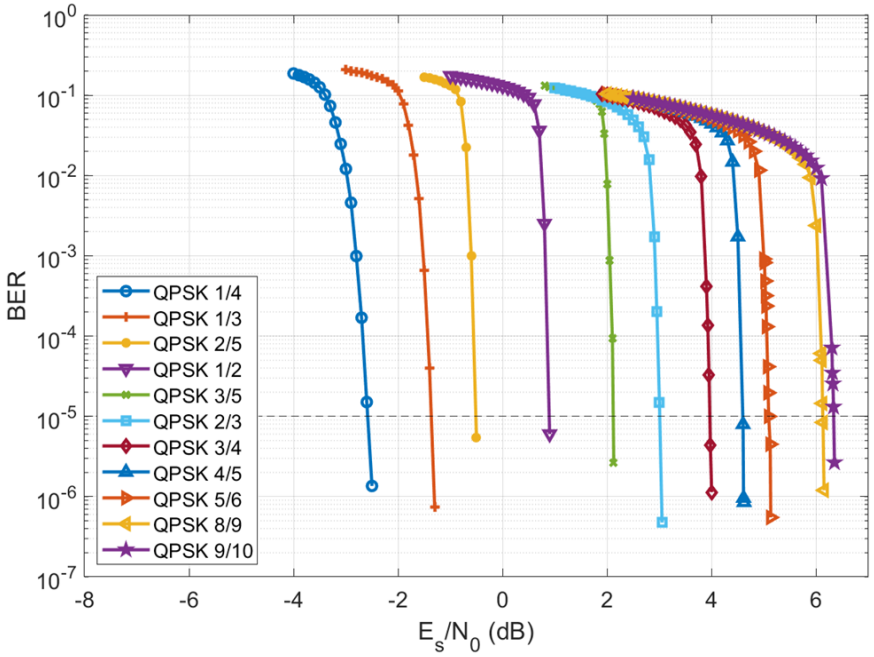


**Figure 2. BER vs $E_s/N_0$ for DVB-S2 Under AWGN with QPSK and Different LDPC Code Rates**

### 3.2 Flat Rayleigh Fading Channel Model

Channel attenuation was measured in 2019 using the AFRL/RV W/V-band Terrestrial Link Experiment (WTLE) test range that is in Albuquerque, New Mexico. Data was measured at 72 GHz (in the V-band). This represents a line-of-sight (LOS), additive white Gaussian noise (AWGN) environment. No channel fading was included in the channel attenuation measurement data. Hence, the channel attenuation data represents the attenuation due to the path loss and

weather conditions. Yet, it is traceable to a W/V-band frequency band, which is statistically different than lower frequency bands. Figure 3 graphically presents the WTLE test setup. The propagation path was approximately 23.5 km through the lower troposphere, which is much more challenging than a typical ground-to-satellite propagation path. Figure 4 presents the time-series of receive power during 2019. Loss of date due to maintenance events is indicated in red. Drops in received signal power are attributable to clouds and precipitation occurring along the propagation path.

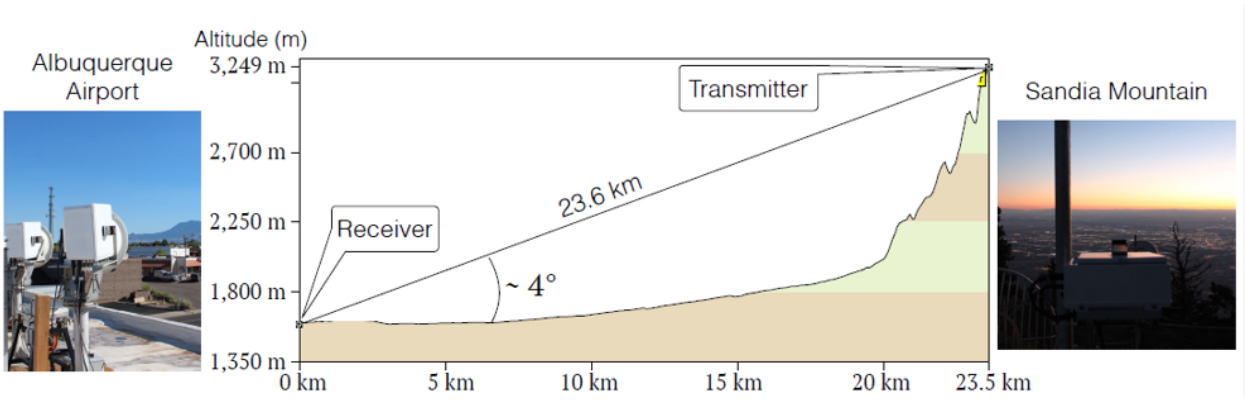


**Figure 3. WTLE Test Range Setup for Measuring Attenuation Statistics for Channel Modeling**

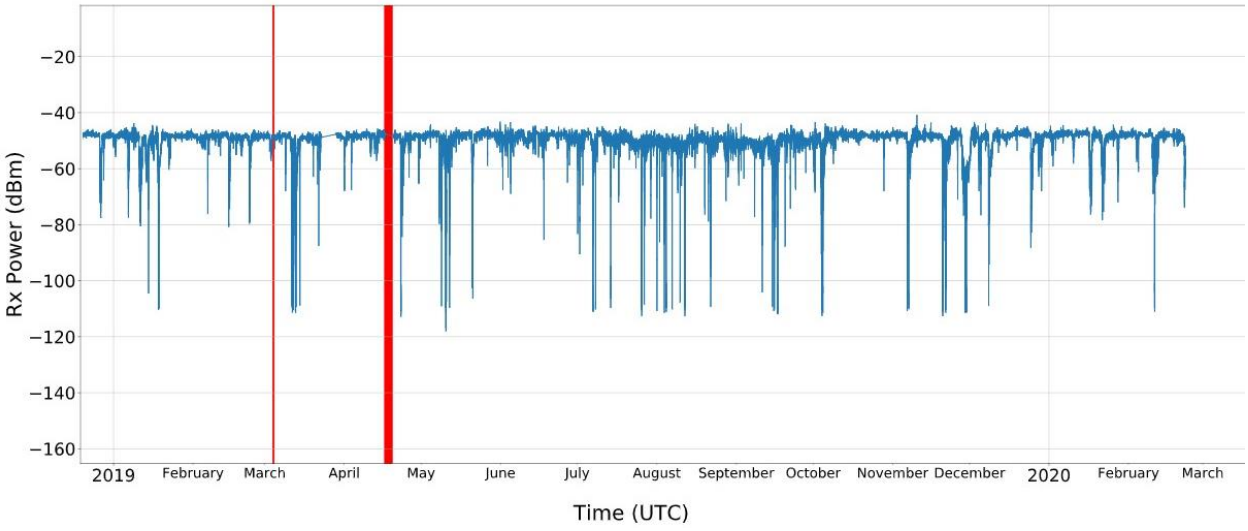


**Figure 4. Received Power Data Obtained in 2019 from WTLE**

For a communications system, the best ACM mode would be implemented based on the W/V-band channel attenuation conditions to maximize the overall bandwidth efficiency (denoted as η).

As noted previously, each ACM mode has different bandwidth efficiencies (bits/s/Hz) and requires different signal-to-noise ratios (SNRs) to achieve a certain performance. In practice, the desirable bit error rate (BER) should be less than or equal to $10^{-5}$ (1 error per 100,000 bits).

However, as shown in Figure 5 (QPSK), Figure 6 (8PSK), Figure 7 (16PSK), and Figure 8 (32PSK), the DVB-S2 modulation methods perform poorly (i.e., BER $\approx 10^{-2}$) under a NLOS, memoryless, flat, and no Doppler shift Rayleigh fading environment. Consequently, the bandwidth efficiency (BWE) of the DVB-S2 protocol under Rayleigh fading would be unsatisfactory. Therefore, the probability of bit error, $P_b = 10^{-2}$ (1 error per 100 bits) is used instead of $P_b = 10^{-5}$ in subsequent computations of bandwidth efficiency.

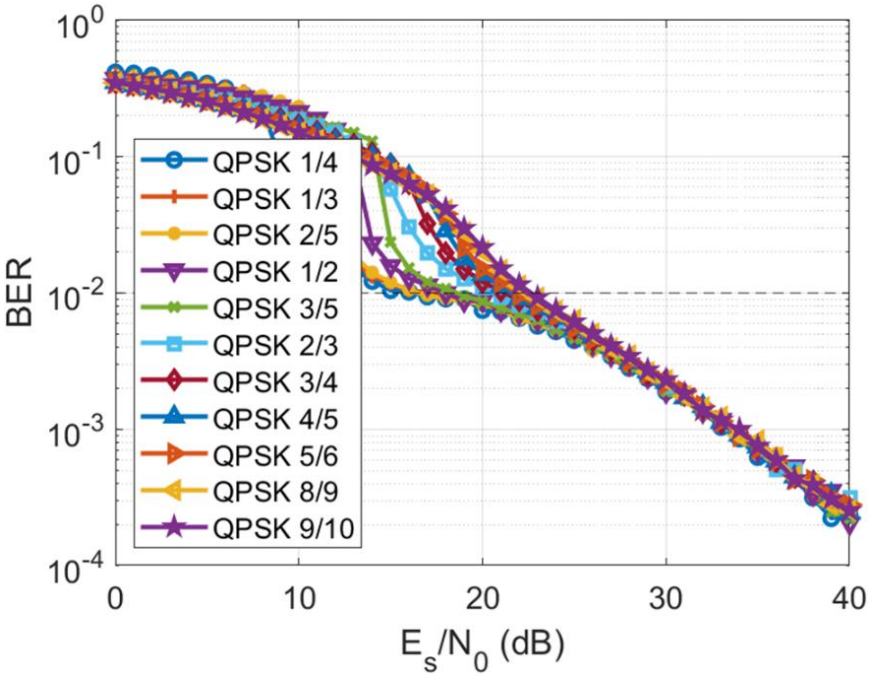


**Figure 5. BER vs $E_s/N_0$ for DVB-S2 Under Flat Rayleigh Fading with QPSK and Different LDPC Code Rates**

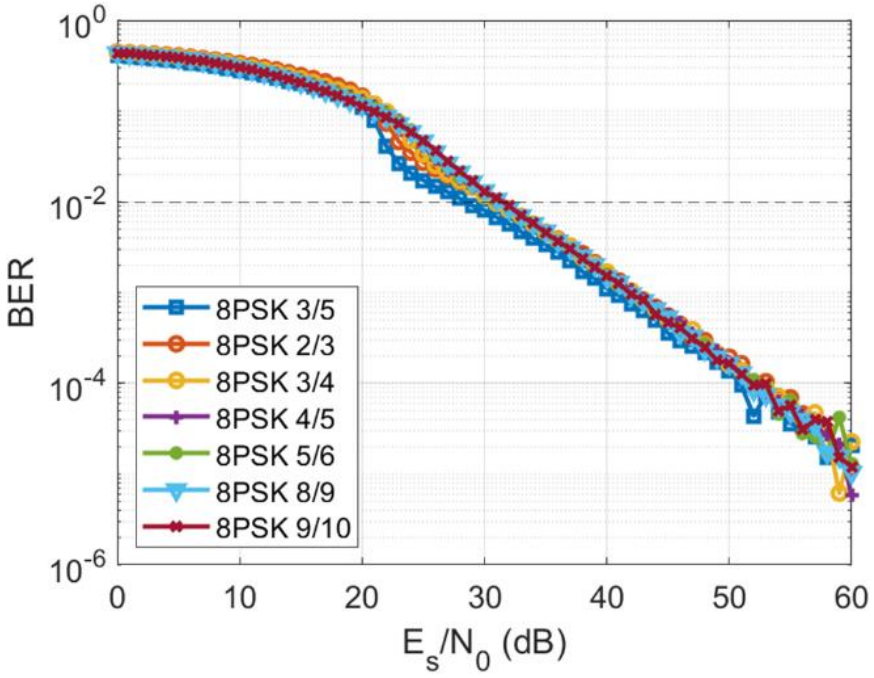


**Figure 6. BER vs *Es*/$N_0$ for DVB-S2 Under Flat Rayleigh Fading with 8PSK and Different LDPC Code Rates**

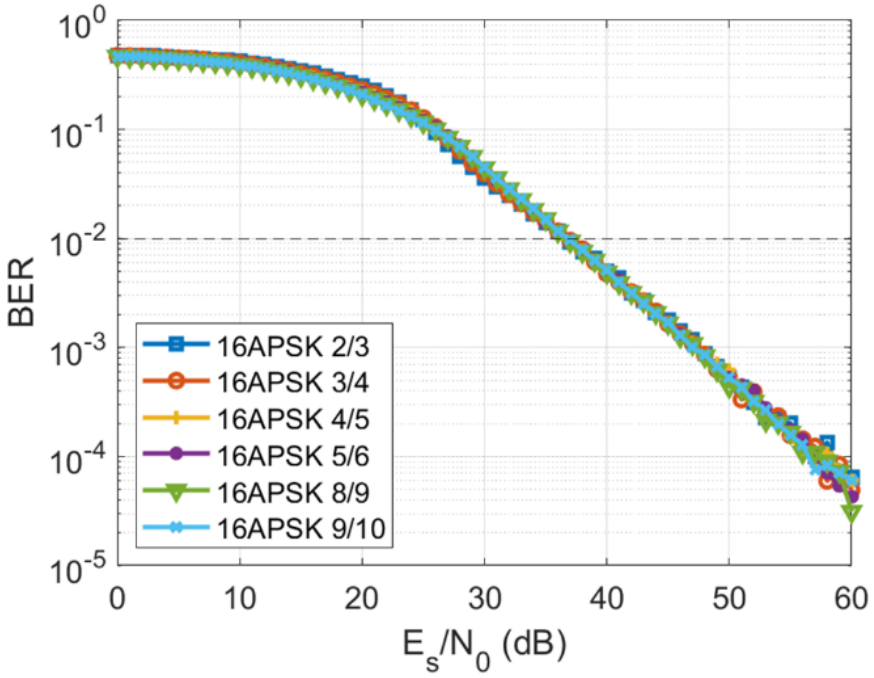


**Figure 7. BER vs $E_s/N_0$ for DVB-S2 Under Flat Rayleigh Fading with 16PSK and Different LDPC Code Rates**

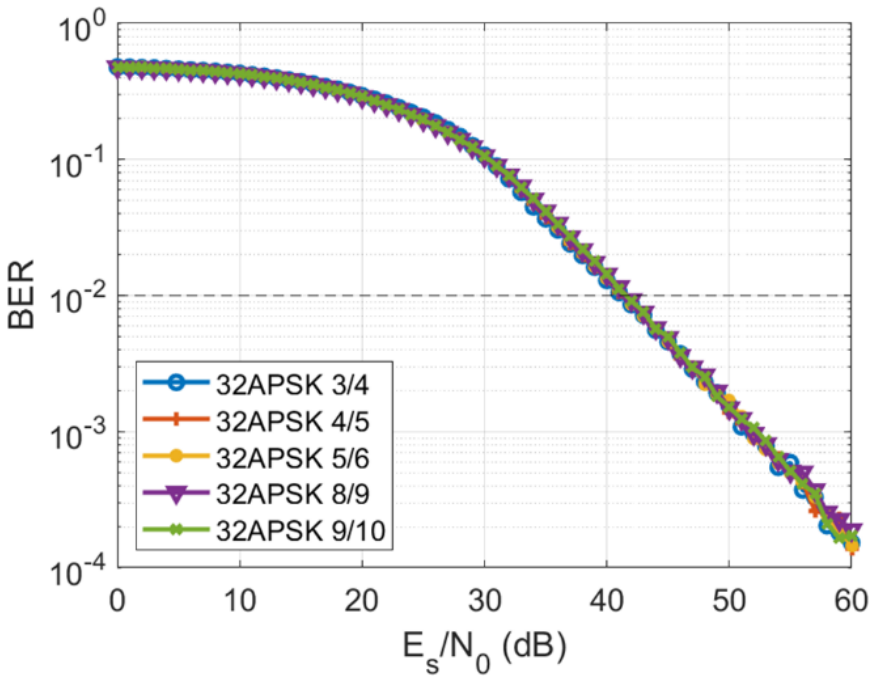


**Figure 8. BER vs $E_s/N_0$ for DVB-S2 Under Flat Rayleigh Fading with 32PSK and Different LDPC Code Rates**

The non-line-of-sight (NLOS), memoryless, flat, no Doppler frequency shift Rayleigh fading channel coefficient is randomly generated by summing the in-phase $h_c$ and quadrature phase $h_s$ Gaussian random variables in the complex domain with each mean zero and variance 1/2 as

$$h(t) = h_c(t) + jh_s(t). \tag{2}$$

Then, the transmitted symbol signal $s(t)$ at time $t$ (i.e., the modulated signal using the LDPC FEC encoded bits) is multiplied by the fading coefficient, $h(t)$. Thermal noise, $n(t)$, is added (zero mean, unity variance). Therefore, the received signal $r(t)$ is:

$$r(t) = h(t)s(t) + n(t). \tag{3}$$

We assume that the Rayleigh fading channel coefficient is perfectly estimated. Then, the received signal is demodulated before LDPC decoding using the maximum ratio combining (MRC):

$$h^*(t)r(t) = h^*(t)h(t)s(t) + h^*(t)n(t) \tag{4}$$

which is equivalent to

$$\frac{r(t)}{h(t)} = s(t) + n(t)/h(t). \tag{5}$$

The corresponding MATLAB source code is given in the Appendix 1 (code requires the Communications Toolbox). The "modOut" variable in line 3 or line 5 (depending upon the modulation order size) represents the modulated symbol after LDPC encoding for a given code rate and the DVB-S2 specific interleaver structure. The "chanOut2" in line 11 represents the

demodulated symbol in Eq. (5) using the Rayleigh fading channel coefficient $h$ in line 9. The complex Gaussian random variable $h$ of mean zero and variance 1 (i.e., the fast Rayleigh fading coefficient $h$) is generated every symbol. Then, the DVB-S2 algorithm is applied for symbol demodulation, LDPC decoding, de-interleaver, and de-packetizing. The BCH is common, and hence used. Thus, the BER in this report represents the decoded BER after the LDPC decoding.

The post-Rayleigh received signal is demodulated, deinterleaved, and decoded. The $E_s/N_0$ is measured at $P_b = 10^{-2}$ instead $P_b = 10^{-5}$. Finally, the data is reconstructed in sequence. The LDPC decoding algorithm runs at 50 iterations at each ACM mode to obtain an average measured $E_s/N_0$.

For example, Figure 5 shows simulation BER versus $E_s/N_0$ results for QPSK. Observe that due to the small-scale Rayleigh fading, the BER is degraded significantly, compared the AWGN case in Figure 2. The ACM cannot be applied at $P_b = 10^{-5}$ BER because all ACM modes show almost the same BER near $E_s/N_0 = 53$ dB. The LDPC decoder shows decoding failure between $E_s/N_0 = 20$ dB and 53 dB.

Table 1 presents the required $E_s/N_0$ for each ACM for $P_b = 10^{-2}$. ACM modes are listed from the lowest $E_s/N_0$ to the highest. Note that the highest bandwidth efficient ACM mode is the worst energy-efficient ACM mode, and vice versa. The ACM mode with the highest required $E_s/N_0$ is designated as mode index $i = 0$, because it is the highest bandwidth efficient ACM mode. The ACM mode with the lowest required $E_s/N_0$ is designated $i = 27$.

The BWE $\eta_i$ of ACM mode $i$ is also decreasing as $i$ increases in general, and is found as

$$\eta_i = R_c(i)\log_2 M(i) \quad \text{(bits/s/Hz)}, \tag{6}$$

where $R_c(i)$ and $M(i)$ are, respectively, the $i$-th ACM mode's code rate and the number of constellation points. Hence, $\log_2 M(i)$ represents the number of coded bits per symbol transmission, where a symbol takes $T_s$ seconds to transmit. Thus, the BWE (bits/s/Hz) in Eq. (6) is the BWE after normalization with $BW = 1/T_s$ (Hz).

We will now consider the exceedance probability (i.e., $\Pr(R_{RX}(dBm) > p_{RX})$) versus the receive measured power (in dBm) for the WTLE link. The upper case $P_{RX}$ and the lower case $p_{RX}$ represent the received measured power random variable and its realization, respectively.

The lowest and highest measured power were -118 dBm and -40 dBm, respectively, which correspond to 78 dB and 0 dB of channel attenuation. The highest received power (-40 dBm) occurred when channel attenuation was caused by only the free-space path loss, i.e., the signal path was in the line-of-sight, the weather was clear, and the surrounding scattering and fading effects were negligible.

Therefore, the highest ACM mode ($i = 0$, 32APSK 9/10) will be assigned under AWGN when attenuation is 0 dB. The next highest ACM mode (32APSK 8/9) will be assigned under AWGN if the attenuation is between 0 dB and 0.085 dB -- from the last column in Table 1. If the channel attenuation is between 0.085 dB and (0.085 + 0.155 = ) 0.240 dB, then the next highest ACM mode (32APSK 5/6) will be assigned under AWGN, and so on.

**Table 1. Required $E_s/N_0$ at $P_b = 10^{-2}$ and Bandwidth Efficiency Under Flat Rayleigh Fading and Link Margin of 25.871 dB**

| Mode index $i$ | ACM mode $i$ | Required $(E_s/N_0)_i$ $dB$ at $P_b = 10^{-2}$ | $\eta_i = R_c log_2 M(i)$ $\left(\frac{bps}{Hz}\right)$ | $\Delta(E_s/N_0)_i = (E_s/N_0)_{i-1} - (E_s/N_0)_i$ $dB$ | $x_i = (E_s/N_0)_0 - (E_s/N_0)_i$ $dB$ |
|---|---|---|---|---|---|
| 27 | QPSK 1/4 | 16.00 | 0.500 | 0.100 | 25.170 |
| 26 | QPSK 2/5 | 16.600 | 0.800 | 0.650 | 25.070 |
| 25 | QPSK 1/3 | 17.250 | 0.667 | 0.750 | 24.420 |
| 24 | QPSK 1/2 | 18.000 | 1.000 | 0.600 | 23.670 |
| 23 | QPSK 3/5 | 18.600 | 1.200 | 1.900 | 23.070 |
| 22 | QPSK 2/3 | 20.500 | 1.333 | 0.750 | 21.170 |
| 21 | QPSK 3/4 | 21.250 | 1.500 | 0.350 | 20.420 |
| 20 | QPSK 4/5 | 21.600 | 1.600 | 0.300 | 20.070 |
| 19 | QPSK 5/6 | 21.900 | 1.667 | 0.700 | 19.770 |
| 18 | QPSK 8/9 | 22.600 | 1.778 | 0.100 | 19.070 |
| 17 | QPSK 9/10 | 22.700 | 1.800 | 5.800 | 18.970 |
| 16 | 8PSK 3/5 | 28.500 | 1.800 | 2.320 | 13.170 |
| 15 | 8PSK 3/4 | 30.820 | 2.250 | 0.230 | 10.850 |
| 14 | 8PSK 5/6 | 31.050 | 2.500 | 0.010 | 10.620 |
| 13 | 8PSK 2/3 | 31.060 | 2.000 | 0.220 | 10.610 |
| 12 | 8PSK 8/9 | 31.280 | 2.667 | 0.220 | 10.390 |
| 11 | 8PSK 9/10 | 31.500 | 2.700 | 5.152 | 10.170 |
| 10 | 16APSK 5/6 | 36.652 | 3.333 | 0.001 | 5.018 |
| 9 | 16APSK 2/3 | 36.653 | 2.667 | 0.003 | 5.017 |
| 8 | 16APSK 4/5 | 36.656 | 3.200 | 0.064 | 5.014 |
| 7 | 16APSK 8/9 | 36.720 | 3.556 | 0.033 | 4.950 |
| 6 | 16APSK 3/4 | 36.753 | 3.000 | 0.087 | 4.917 |
| 5 | 16APSK 9/10 | 36.840 | 3.600 | 4.390 | 4.830 |
| 4 | 32APSK 4/5 | 41.230 | 4.000 | 0.020 | 0.440 |
| 3 | 32APSK 3/4 | 41.250 | 3.750 | 0.180 | 0.420 |
| 2 | 32APSK 5/6 | 41.430 | 4.167 | 0.155 | 0.240 |
| 1 | 32APSK 9/10 | 41.585 | 4.500 | 0.085 | 0.085 |
| 0 | 32APSK 8/9 | 41.670 | 4.444 | n/a | 0.000 |

Hence, the received power random variable $P_{RX}$ (dBm) is converted to the attenuation random variable $X$ (in dB). This is accomplished by subtracting the observed power level from an offset received power value (-40 dBm for this study) to achieve an attenuation, $X$ using the relation:

$$X = -40 - P_{RX}. \tag{7}$$

The exceedance probability of the measured power $P_{RX}$ and the cumulative distribution function (CDF) of the attenuation random variable $X$ can be related using Eq. (7) as:

$$\Pr(P_{RX} \geq p_{RX}) = \Pr(P_{RX} = -X - 40 \geq p_{RX}) = \Pr(X \leq x = -10 - p_{RX}) = F_X(x) \tag{8}$$

which is the CDF of the attenuation random variable $X$. This CDF is shown in Figure 9.

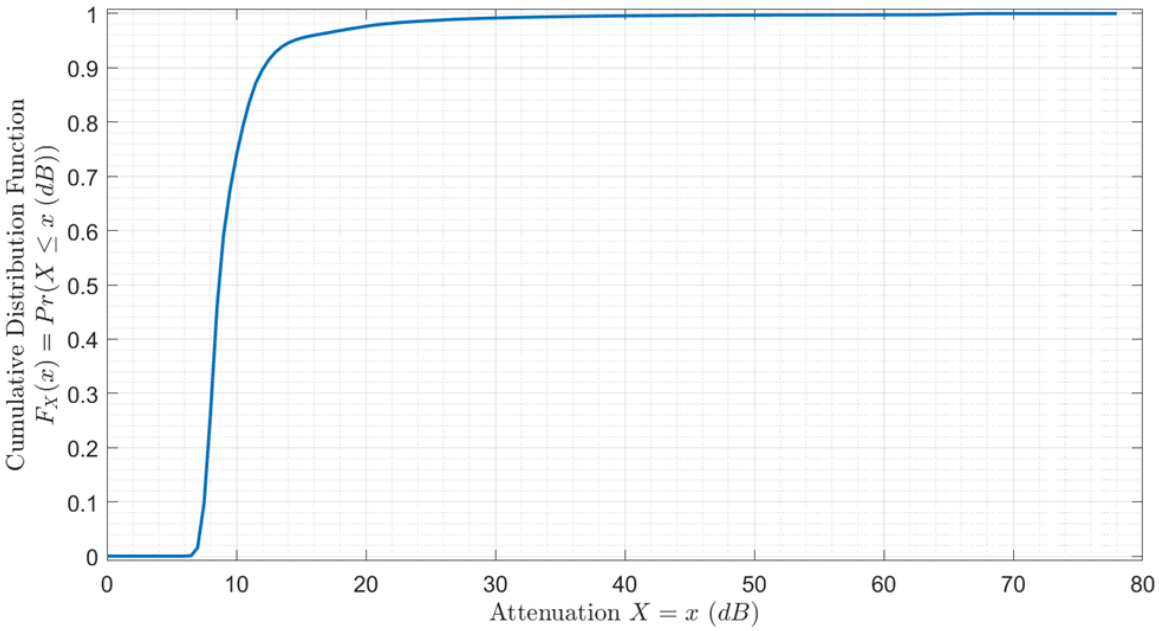


**Figure 9. CDF $F_X(x)$ of Attenuation Random Variable $X$**

Before applying the CDF of the attenuation, the difference of the required $E_s/N_0$ at $P_b = 10^{-2}$ between the ACM mode $i$-1 and $i$, except for ACM mode $i = 0$, is computed using the third column of Table 1 and is listed in the fifth column, $i = 1,...,27$:

$$\Delta(E_s/N_0)_i = (E_s/N_0)_{i-1} - (E_s/N_0)_i. \tag{9}$$

This difference is used to find the best ACM mode from the current ACM mode, $i$, depending on the attenuation under AWGN. It is desirable to use an ACM mode of a lower index for a higher BWE, if the received SNR meets the minimum required SNR in Table 1. Refer to the fourth column of Table 1, which lists the BWE $\eta_i$ of each ACM mode $i$.

The signal to noise ratio (SNR) for the channel is not available because it was not measured. Only the CDF of the measured attenuation is available. Hence, the attenuation random variable *X* must be used to compute the BWE of the terrestrial W/V-band link.

Note that the sum of the differences $\Delta(E_s/N_0)_i$ in Eq. (9) is just the difference between the first term and the last term in the sum, i.e., $\sum_{j=1}^{i} \Delta(E_s/N_0)_j = (E_s/N_0)_0 - (E_s/N_0)_i$. This sum corresponds to the cumulative attenuation from the ACM mode 0 to the ACM mode *i*. Therefore, this sum also indicates which ACM mode is the best to use for a given attenuation *X*. In other words, if the attenuation *X* is:

$$(E_s/N_0)_0 - (E_s/N_0)_{i-1} \leq X < (E_s/N_0)_0 - (E_s/N_0)_i \tag{10}$$

i.e., if

$$\sum_{j=1}^{i-1} \Delta(E_s/N_0)_j \leq X < \sum_{j=1}^{i} \Delta(E_s/N_0)_j \tag{11}$$

for $i = 1, \ldots, 27$, then the radio transceiver will adjust ACM mode *i*.

In Table 1, the sixth column, lists the $x_i = (E_s/N_0)_0 - (E_s/N_0)_i$ in dB for the DVB-S2 system to change the ACM mode *i* when the attenuation *X* meets the criteria of the inequality in Eq. (10) and the link margin $x_{LM} = 0$ dB. The system will optimize the BWE by finding the ACM mode *i* corresponding to the attenuation *X* using Eq. (10).

To find the probabilities $p_i$ for ACM mode *i* under AWGN, we can use the measured attenuation CDF in Figure 9 to provide the information necessary to compute the $p_i$ for each ACM mode *i*:

$$p_i = Pr(ACM_i \; used) = F_X(X = x_i) - F_X(X = x_{i-1}) \tag{12}$$

for *i* = 1, …, 26, where $F_X(x_i)$ is defined in Eq. (8). This is because the ACM mode *i* will be selected if the attenuation random variable *X* satisfies Eq. (10).

From the prior study, we observed that the highest ACM mode under AWGN is 32APSK9/10 and required the received SNR $E_s/N_0$ = 15.799 dB at $P_b = 10^{-5}$ BER. Hence, the nominal operating received SNR is assumed to be $E_s/N_0$ = 15.799 dB.

However, under Rayleigh fading, the received required SNR should be $E_s/N_0$ = 41.670 dB, even at $10^{-2}$ BER from Table 1. Therefore, to support the ACM mode 0, i.e., 32APSK9/10 of the highest BWE under Rayleigh fading, it will require additional transmitted power of 41.67 - 15.799 = 25.871 dB. If the extra link margin $x_{LM}$ is 25.871 dB, then the highest ACM mode 32APSK9/10 can be supported with probability $p_0$. The probability $p_0$ can be obtained from the CDF of the attenuation in Figure 9, e.g., $p_0 \approx 0$ at attenuation *X* = 0 dB. However, the link margin of 25.871 dB is hard to achieve in practice. Probability $p_i$ of other ACM mode *i* can be obtained from Figure 9 and Eq. (12).

The average BWE of the W/V band system in bits/s/Hz is computed as:

$$E[\eta] = (1 - P_b) \sum_0^{27} n_i p_i \text{ (bits/s/Hz)} \tag{13}$$

where $(1 - P_b)$ is multiplied to consider only the bits delivered with no errors when a best ACM mode in DVB-S2 is transmitted depending on the channel attenuation.

Finally, each of the W-band and the V-band channels have contiguous BW = 5 GHz, and the W- and V-bands occupy 81-86 GHz and 71-76 GHz frequency bands, respectively. Hence, the BW=5 GHz is multiplied to the BWE in Eq. (13) to find the average BWE in bits/s and rewritten as

$$E[BWE] = BW \cdot E[\eta] \text{ (bits/s)}. \quad (14)$$

The required SNR $E_s/N_0$ for each ACM mode to achieve $BER \leq 10^{-2}$ was found through the DVB-S2 system under a Rayleigh channel environment. Figure 5 shows the BER versus $E_s/N_0$ for QPSK ACM modes. A dotted line passing through $BER = 10^{-2}$ is shown in each figure, and the corresponding required SNR $E_s/N_0$ for each mode is listed in the third column of Table 1. The bandwidth efficiencies and differences in required $E_s/N_0$ are also listed in Table 1 to relate to the CDF $F_X(x) = \Pr(X \leq x)$ of the attenuation random variable X in Figure 9. When the link margin is 25.871 dB, each $ACM_i$ mode is ranked from the highest required $E_s/N_0$ ACM mode of $i = 0$ at $P_b \leq 10^{-2}$ to the lowest for ACM mode of $i = 27$ in Table 1. Under Rayleigh fading, the ACM mode 32APSK at code rate 8/9 requires a higher SNR than the highest ACM mode 32APSK at code rate 9/10, and the lowest is QPSK at code rate 1/4. Hence, the highest 32APSK at code rate 9/10 can still be used at the attenuation equal to the link margin.

Typically, a higher ACM mode requires a higher cost, i.e., a higher receive SNR $E_s/N_0$ to achieve $P_b \leq 10^{-2}$, even though it shows a higher BWE. Hence, it will be desirable to transmit the highest ACM mode 32APSK (9/10) at attenuation $X = x_{LM}$ under clear weather conditions. Then, for further attenuation from $x_{LM}$ due to rain, the next highest ACM mode is desirable to be transmitted with $P_b \leq 10^{-2}$.

Two cases were considered for bandwidth efficiency computation. Case A begins at the highest received power -40 dBm (i.e., $x_{LM} = 0$ dB) and Case B begins at -50 dBm (i.e., $x_{LM} = 10$ dB). This further attenuation $x_i$ can be computed using $x_i - x_0 = (E_s/N_0)_0 - (E_s/N_0)_i$, and $x_i - x_{LM}$, and is associated with the ACM mode $i$. For example, in Case A, $x_i - x_{LM} = 0$ dB and $x_{i=1} - x_0 = (E_s/N_0)_0 - (E_s/N_0)_{i=1}$dB from Table 1. Hence, $x_{i=1} = x_0 + 0.085\,dB = 0.085\,dB$.

For Case A of 0 dB link margin, even the lowest ACM mode QPSK 1/4 required $E_s/N_0$ of 16.500 dB at $BER = 10^{-2}$ under Rayleigh fading, which is higher than the highest ACM mode 32APSK 9/10 at $BER = 10^{-5}$ under AWGN that requires an $E_s/N_0$ of 15.799 dB. It is assumed that the nominal operating SNR is set to the highest ACM mode 32APSK 9/10 at $BER = 10^{-5}$ under AWGN of $E_s/N_0$ equal to 15.799 dB. If the channel attenuation $X$ in dB is positive, then the system looks for an ACM mode that requires $E_s/N_0 \leq 15.799$ dB. Unfortunately, for Case A of 0 dB link margin, the system cannot find any ACM mode under Rayleigh fading and hence the BWE is equal to zero. Table 2 provides the BWE of 0 for Case A under Rayleigh fading where no ACM modes can be applied. Table 3 provides the corresponding BWE of 9.449 Gbits/s for Case A under AWGN, where all ACM modes can be applicable.

**Table 2. BWE Results Under Flat Rayleigh Fading with BW=5 GHz**

| Case | $E[\eta] \times BW$ (Gbps) per antenna beam | Highest Probability ACM Mode ($R_c$) |
|---|---|---|
| A | 0 | n/a |
| B | 0.0005 | QPSK (2/5) |

**Table 3. BWE Results Under AWGN with BW=5 GHz**

| Case | $E[\eta] \times BW$ (Gbps) per antenna beam | Highest Probability ACM Mode ($R_c$) |
|---|---|---|
| A | 9.449 | 8PSK (5/6) |
| B | 21.371 | 32APSK (9/10) |

For Case B, the link margin $x_i - x_{LM} = 10$ dB and the nominal operating SNR under AWGN is 15.799 dB for the highest ACM mode 32APSK 9/10 rate. Hence, the system can support the ACM modes with the maximum required SNR up to 25.799 dB including 10 dB link margin. Hence, the highest ACM mode in Table 1 under Rayleigh fading is the QPSK 9/10 at $BER = 10^{-2}$ since it's required $E_s/N_0$ is 22.700 dB which is less than 25.799 dB. The ACM can be used between QPSK 1/4 and QPSK 9/10 and the remaining ACM modes; 8PSK, 16APSK, 32APSK cannot be supported. The QPSK 1/4 has the highest probability of 0.00009349 and will be transmitted at attenuation $X = x_{LM} = 10$ dB from the nominal operating SNR of 15.799 dB. The BWE is calculated in Table 3 for Case B using Eq. (12) and Eq. (13). Data also shows that the product of bandwidth efficiency times the probability of ACM mode *i* being used, i.e., $\eta_i p_i$, is the highest at the ACM mode QPSK (2/5). This is why the average BWE for Case B is higher than that for Case A.

When all $p_i$ are added up for each ACM mode, the sum should be equal to 1. The attenuation index range could be used as a sliding rule along the CDF attenuation curve in Figure 9. The probability mass function (pmf) for each ACM mode can be quickly calculated, and the highest probability can be found to change the ACM that achieves the best BWE.

In Table 2 the average BWE for each case in (Gbits/s) per antenna beam, the highest probability ACM mode, and $R_c$ are shown. Observe that the higher link margin yields a higher BWE. However, this requires a higher cost, e.g., a higher transmitting power, a larger antenna size, and a lower noise figure, etc. Case A is the worst. Case B is the most reasonable out of two cases for practical application, but the BER wasn't sufficiently large enough to reach $10^{-5}$and it makes no difference in $E_s/N_0$ among the different ACM modes.

*Remarks*: The BWE results in Table 2 were obtained for the DVB-S2 under a memoryless, no Doppler frequency shift, flat Rayleigh fading channel environment. If the channel is an AWGN with no Rayleigh fading, then the ACM mode $i$ = 0, i.e., 32APSK 9/10 will require the received $E_s/N_0 \geq 15.799$ dB to achieve $BER = 10^{-5}$ from BER curves in Figure 2 and other BERs for 16APSK and 32APSK. However, if the channel is under a Rayleigh fading, then the ACM mode $i$ = 0, i.e., 32APSK 9/10 will require much higher received $E_s/N_0 \geq 27.3$ dB to achieve a worse $BER = 10^{-5}$ from Table 1 and Figure 5. Hence, the transmitted signal power under the Rayleigh fading channel should be at least 12.5 dB higher than that under the AWGN. Furthermore, the BER under the Rayleigh fading is three decades worse than that under the AWGN.

### 3.3 Frequency Selective Rayleigh Fading Channel Model

In the previous section, bandwidth efficiency analysis was presented under a single multipath Rayleigh fading channel using the DVB-S2 system and measured W/V-band channel attenuation data. This analysis is expanded in this section to a shortened DVB-S2 system and 5G Orthogonal Frequency Division Multiplexing (OFDM) communication by considering a multiple multipath Rayleigh fading channel called a ***frequency selective fading*** channel. Since such a fading channel in the frequency response is not flat over the broad data bandwidth, the signal data is degraded in frequency selective way.

Application of OFDM for digital transmission improved performance against such severe multipath fading environments, especially when the transmission data rate is much higher than the channel coherence bandwidth. The channel coherence bandwidth is inversely proportional to the multipath delay spread. In this work, the multipath delay spread was assumed to be three sample time units (i.e., three data symbol time intervals). Two multi-path profiles were considered with seventy percent of the received signal power occurred at the first multipath path and thirty percent of the received power at the second path. Each path was modeled as a Rayleigh fading channel.

The OFDM has been used in 4G/5G mobile communications to protect the data of high data rate under such a severe frequency selective fading channel. However, the OFDM is not included in the existing DVB-S2 standard yet for satellite communications. This is probably because the LOS is typically assumed in a typical satellite communication environment. However, the received signal can be under NLOS situations, e.g., the receivers inside a building or in a heavy forest or in a heavy thunderstorm. In addition, it is under discussion in the 3GPP society that the future 6G mobile communication system should include satellite communication service. Then, the W/V band can be a possible candidate for 6G terrestrial communications with W/V-band satellite communication links. Therefore, it is worthwhile to investigate the effect of the frequency selective NLOS fading channel environment on the communication systems.

The corresponding MATLAB source code is given in Appendix 2 (code requires the Communications Toolbox). The “modOut” variable in line 12 or 14 represents the modulated symbol after low density parity check encoding for a given code rate, and the DVB-S2 specific interleaver structure will need to enter a serial to parallel conversion. Depending on the size of the

"modOut" column matrix of QPSK, 8PSK, 16APSK, and 32APSK, it is divided into 1024 subcarriers to pass through the serial to parallel conversion to be processed into the OFDM modulator shown in Figure 10. In this work, the fast Fourier transform (FFT) of size 1024 was used. In other words, the column matrix of "modOut" was a matrix size 1024 by the number of divisible rows of 1024 subcarriers. Since the DVB-S2 frame size is not a multiple of 1024, the final column was padded by zero for the remainder portion.

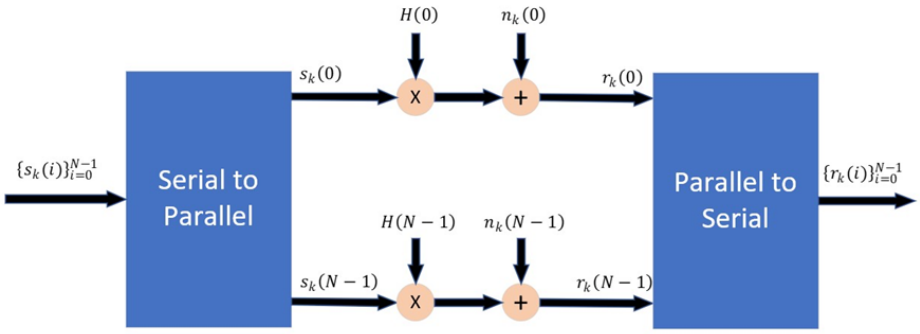


**Figure 10. OFDM Channel Frequency Response**

To generate a fading channel of channel impulse response (CIR) $h(n)$, an individual fading coefficient for each multipath was randomly generated and then combined to generate an overall fading channel. For example, the amplitude of the first multipath fading coefficient represented by $h_0$ was a Rayleigh distributed with power 0.7 and delay $\tau_0 = 0$ unit sample time. In this work, a unit sample time interval was equal to the transmitted symbol time interval. The amplitude of the second multipath fading coefficient represented by $h_1$ was also a Rayleigh distributed variable with power 0.3 and delay $\tau_1 = 3$ unit sample time. The total number of multipaths was assumed to be $L = 2$ in this model. A general CIR can be written as

$$h(\mathrm{n}) = h_0\delta(n-\tau_0) + h_1\delta(n-\tau_1) + \cdots + h_{L-1}\delta(n-\tau_{L-1}). \quad (15)$$

Each multipath coefficient needs to generate its real component and imaginary component, then sum them to get a fading coefficient for each path as

$$h(n) = h_r(n) + jh_i(n) \quad (16)$$

where $h_r(n)$ and $h_i(n)$ are Gaussian distributed random variables with mean zero and variance $\sigma^2(n)/2$, $\sigma^2(n=0) = 0.7$, $\sigma^2(n=3) = 0.3$ and $\sigma^2(n \neq 0,3) = 0$. The power of each fading coefficient is equal to

$$\sigma^2(n) = \text{power of the } n\text{th path}. \quad (17)$$

Lines 18-19 in Appendix 2 show the fading coefficient generation.

Then, the channel frequency response (CFR) $H(i)$ was computed by taking the FFT of $h(n)$. The CFR was multiplied by $s_k(i)$, which is the subcarrier element $i$ of "modOut". Then, an additive Gaussian noise $n_k(i)$ was added to get the received signal symbol $r_k(i)$ as:

$$r_k(i) = H(i)\, s_k(i) + n_k(i), \qquad i = 0, \ldots, N-1\,. \tag{18}$$

To demodulate the $i^{\text{th}}$ transmitted symbol, $s_k(i)$, which was input to the OFDM, the received symbol $r_k(i)$ was divided by $H(i)$ as $\hat{s}_k(i)$, line 25. Then, the demodulated matrix was converted back into the column matrix for the ACM demodulation chosen by the user, line 27-28:

$$\hat{s}_k(i) = \frac{r_k(i)}{H(i)}, \;\; i = 0, \ldots, (N-1). \tag{19}$$

In Figure 11, Figure 12, Figure 13, and Figure 14, the ACM modes were chosen with low, medium, and high code rates, because the BER curves were so close together within the modulation schemes. The low, medium, and high code rates for modulations schemes were chosen as: QPSK: {1/4, 1/2, 9/10}, 8PSK: {3/5, 3/4, 9/10}, 16APSK: {2/3, 4/5, 9/10}, and 32APSK: {3/4, 5/6, 9/10}. Then, the BER at $10^{-2}$ is taken since $10^{-5}$ BER could not be achieved. It exceeded the SNR beyond the possible power to produce that in practice.

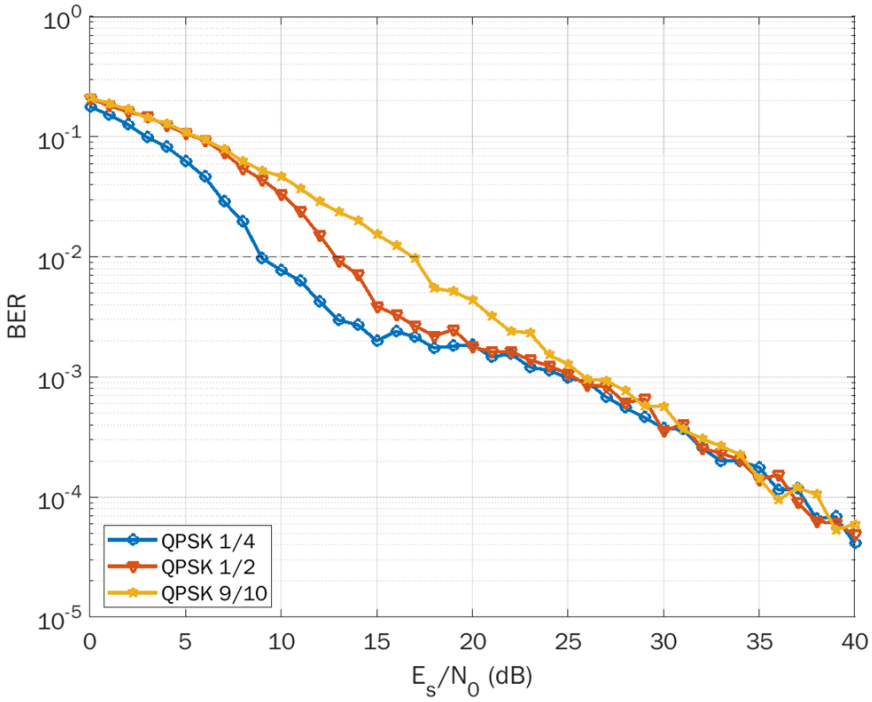


**Figure 11. DVB-S2 QPSK Two Multipath Rayleigh Fading With OFDM**

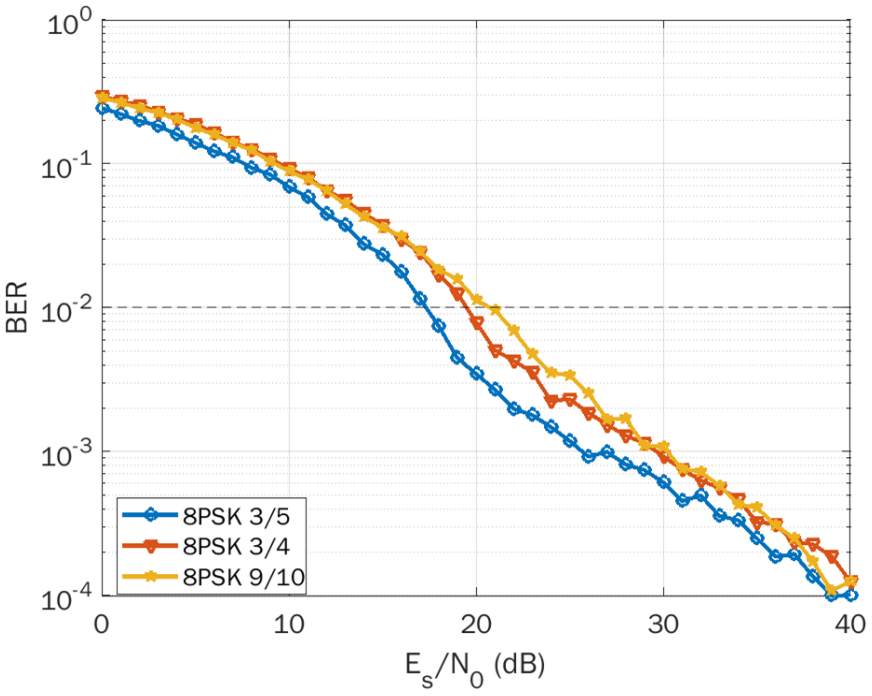


**Figure 12. DVB-S2 8PSK Two Multipath Rayleigh Fading with OFDM**

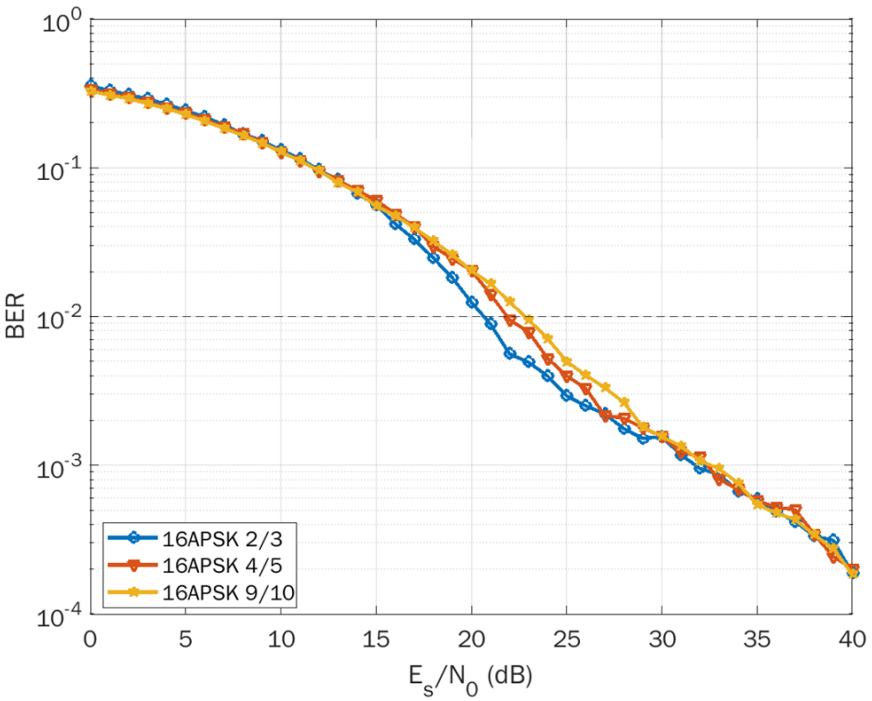


**Figure 13. DVB-S2 16APSK Two Multipath Rayleigh Fading With OFDM**

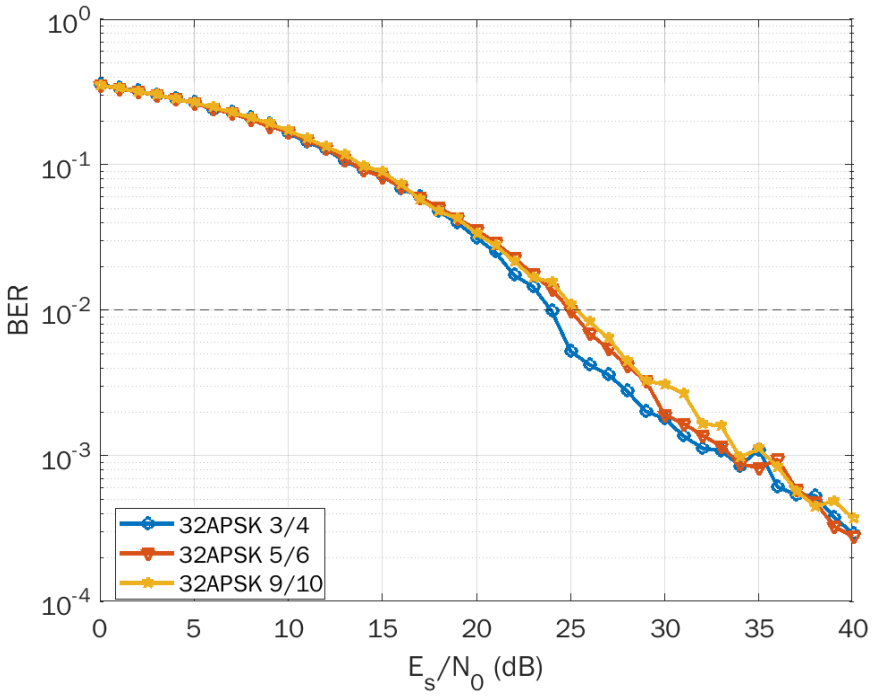


**Figure 14. DVB-S2 32APSK Two Multipath Rayleigh Fading with OFDM**

Figure 11, Figure 12, Figure 13, and Figure 14 show the BERs of the DVB-S2 ACM modes when the OFDM was used under the two-path frequency selective multipath Rayleigh fading channel with 0.7 power at the first and 0.3 power at the second path and four symbol time intervals separation between two path arrival times. On the other hand, Figure 2, Figure 5, Figure 6, Figure 7, and Figure 8 show the BERs of the DVB-S2 ACM modes when the OFDM was not used under the single-path frequency flat multipath Rayleigh fading channel with 1.0 power at the single path. ***From these two BER sets, observe that the OFDM improves the BER significantly by more than 10 dB in SNR, compared to the no OFDM system.*** However, still the BER is much worse than that under the AWGN channel.

In Table 4, each ACM mode's code rate is ranked and the cumulative distribution function (CDF) of the attenuation (in dB) in Figure 9 was applied with the link margin of 0 dB (i.e., Case A). In Table 5, the BWE is listed since it has the highest BWE and 6.62 Gbps rate can be supported per antenna beam with ACM mode of QPSK 1/2 and link margin 16.36 dB.

**Table 4. BWE Results Under Two Multipath Rayleigh Fading Channel and OFDM with BW=5 GHz**

| Mode index $i$ | ACM mode $i$ | Required $(E_s/N_0)_i$ $dB$ at $P_b = 10^{-2}$ | $\eta_i = R_c log_2 M(i)$ $\left(\frac{bps}{Hz}\right)$ | $\Delta(E_s/N_0)_i = (E_s/N_0)_{i-1} - (E_s/N_0)_i$ $dB$ | $x_i = (E_s/N_0)_0 - (E_s/N_0)_i$ $dB$ |
|---|---|---|---|---|---|
| 11 | QPSK 1/4 | 8.96 | 0.50 | 3.89 | 16.36 |
| 10 | QPSK 1/2 | 12.85 | 1.00 | 4.00 | 12.47 |
| 9 | QPSK 9/10 | 16.85 | 1.80 | 0.48 | 8.47 |
| 8 | 8PSK 3/5 | 17.33 | 1.80 | 2.17 | 7.99 |
| 7 | 8PSK 3/4 | 19.5 | 2.25 | 1.16 | 5.82 |
| 6 | 16APSK 2/3 | 20.66 | 2.67 | 0.11 | 4.66 |
| 5 | 8PSK 9/10 | 20.77 | 2.70 | 1.10 | 4.55 |
| 4 | 16APSK 4/5 | 21.87 | 3.20 | 0.94 | 3.45 |
| 3 | 16APSK 9/10 | 22.81 | 3.60 | 1.15 | 2.51 |
| 2 | 32APSK 3/4 | 23.96 | 3.75 | 1.03 | 1.36 |
| 1 | 32APSK 5/6 | 24.99 | 4.17 | 0.33 | 0.33 |
| 0 | 32APSK 9/10 | 25.32 | 4.50 | 0.00 | 0 |

**Table 5. Required $E_s/N_0$ at $P_b = 10^{-2}$ and BWE Under Two Multipath Rayleigh Fading with OFDM and Link Margin of 16.36 dB**

| Case | $E[\eta] \times BW$ $(Gbps)$ per antenna beam | Highest Probability ACM Mode ($R_c$) |
|---|---|---|
| A | 6.62 | QPSK (1/2) |

### 3.4 Flat Rician Fading Channel Model

The objective of this section is to demonstrate how to convert from the set of channel attenuation measurement data obtained under the LOS and AWGN to data rate of a memoryless, line-of-sight, flat, no Doppler, and flat Rician fading channel (i.e., bandwidth efficiency in bits per second per Hz (bits/s/Hz) or bits/s of the channel). This section will take a real channel attenuation measurement data set obtained in 2019 for a W/V-band channel and a practical ACM scheme

called Digital Video Broadcasting - Second Generation (DVB-S2) and will demonstrate steps to compute the BWE of the W/V-band channel under a flat, LOS, memoryless, no Doppler, and Rician fading.

Simulation results of the bit error rate as a function of $E_s/N_0$ for the WTLE channel under a line-of-sight, memoryless, flat, and no Doppler shift Rician fading environment are presented in Figure 15 (QPSK), Figure 16 (8PSK), Figure 17 (16PSK), and Figure 18 (32PSK). The BWE of the DVB-S2 under Rician fading would be satisfactory for QPSK and 8PSK, but unsatisfactory for 16APSK and 32APSK, since the SNR was too large to support the ACM modes. Therefore, $P_b = 10^{-5}$ criterion was used to apply the ACM and BWE computation for QPSK and 8PSK.

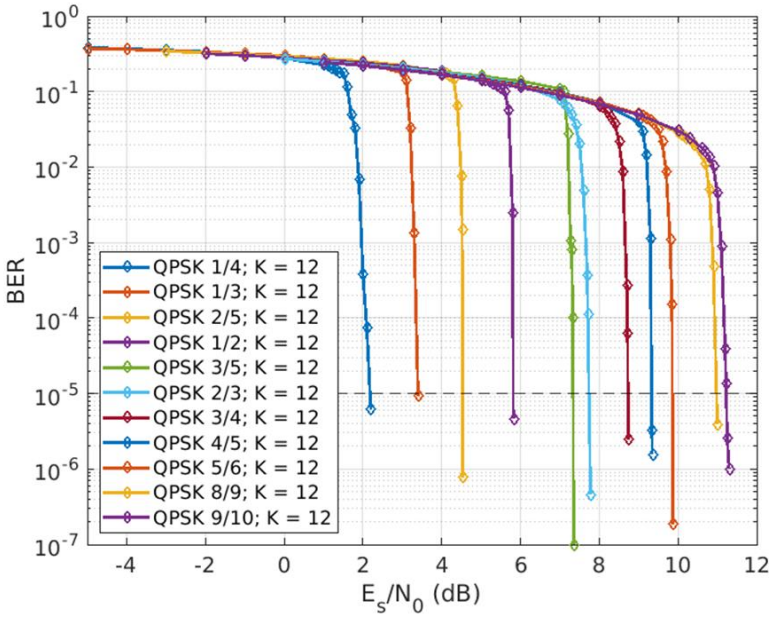


**Figure 15. BER vs $E_s/N_0$ for DVB-S2 Under Flat Rician Fading with QPSK and Different LDPC Code Rates**

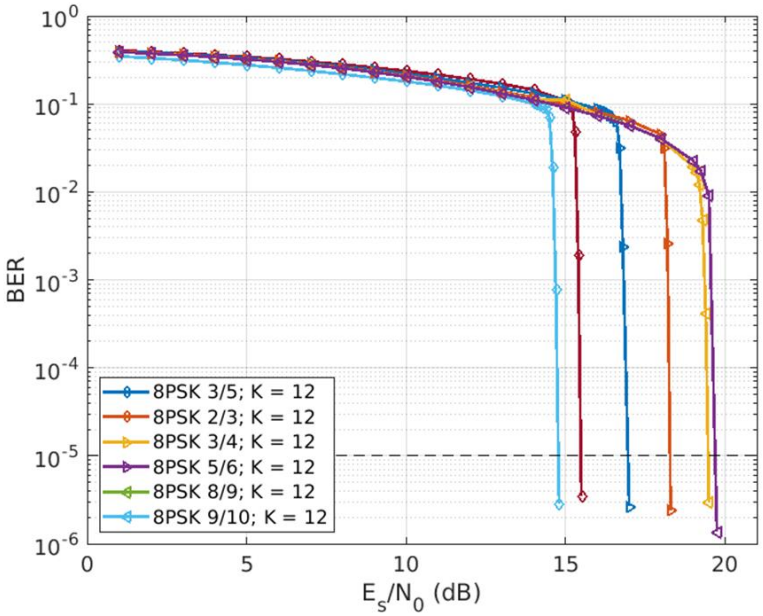


**Figure 16. BER vs $E_s/N_0$ for DVB-S2 Under Flat Rician Fading with 8PSK and Different LDPC Code Rates**

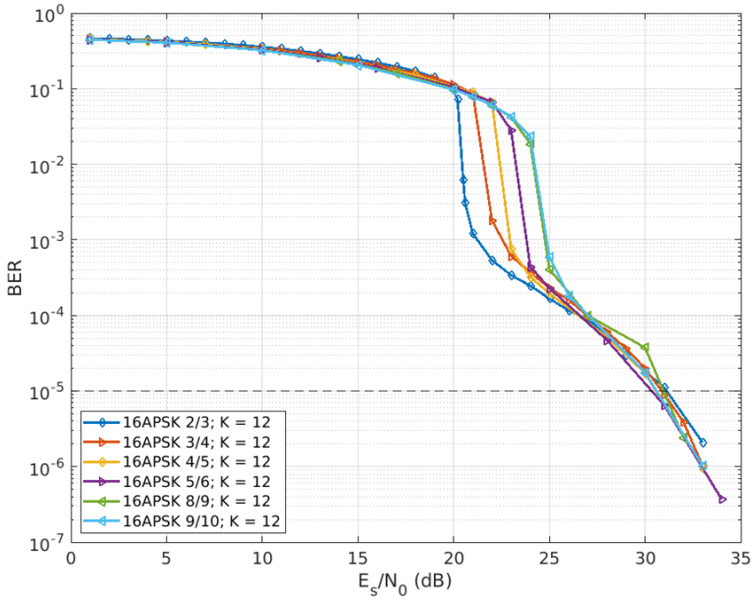


**Figure 17. BER vs $E_s/N_0$ for DVB-S2 Under Flat Rician Fading with 16APSK and Different LDPC Code Rates**

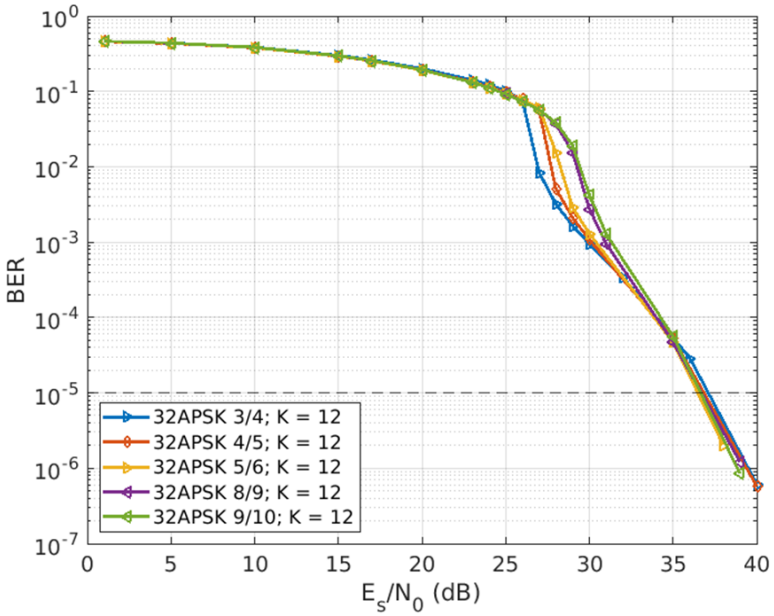


**Figure 18. BER vs $E_s/N_0$ for DVB-S2 Under Flat Rician Fading with 32APSK and Different LDPC Code Rates**

The corresponding MATLAB source code is shown in the Appendix 3. The variable "modOut" in line 7 or 9, depending upon the modulation order size, represents the modulated symbol after LDPC encoding for a given code rate and the DVB-S2 specific interleaver structure. The "chanOut2" in line 14 represents the demodulated symbol in Eq. (5) using the Rician fading channel coefficient $h$ in line 11. The complex Gaussian random variable $h$ of mean zero and variance 1 (i.e., the fast Rayleigh fading coefficient) is generated every symbol. Then, the DVB-S2 algorithm was applied for symbol demodulation, LDPC decoding, de-interleaver, and de-packetizing. The BCH is common, and hence unused. Thus, the BER in this report represents the decoded BER after the LDPC decoding. The post-Rician received signal was demodulated, deinterleaved, and decoded. The $E_s/N_0$ was measured at $P_b = 10^{-5}$. Finally, data was reassembling in sequence. The LDPC decoding algorithm ran at 50 iterations at each ACM mode to obtain an average measured $E_s/N_0$. For example, Figure 15 shows simulation BER versus $E_s/N_0$ results for QPSK ACM mode. Observe that due to the small-scale Rician fading, the BER increased compared to the AWGN case in Figure 2.

Table 6 presents the required $E_s/N_0$ for each ACM for $P_b = 10^{-5}$. ACM modes are listed from the lowest $E_s/N_0$ to the highest. Note that the highest bandwidth efficient ACM mode is the worst energy-efficient ACM mode, and vice versa. The ACM mode with the highest required $E_s/N_0$ is designated as mode index $i = 0$, because it is the highest bandwidth efficient ACM mode. The ACM mode with the lowest required $E_s/N_0$ is designated $i = 27$. The BWE, $\eta_i$, is also decreasing as $i$ increases and defined in Eq. (6).

**Table 6. Required $E_s/N_0$ at $P_b = 10^{-5}$ and BWE Under Flat Rician Fading and Link Margin of 21.401 dB**

| Mode index $i$ | ACM mode $i$ | Required $(E_s/N_0)_i$ $dB$ at $P_b = 10^{-2}$ | $\eta_i = R_c log_2 M(i)$ $\left(\frac{bps}{Hz}\right)$ | $\Delta(E_s/N_0)_i = (E_s/N_0)_{i-1} - (E_s/N_0)_i$ $dB$ | $x_i = (E_s/N_0)_0 - (E_s/N_0)_i$ $dB$ |
|---|---|---|---|---|---|
| 27 | QPSK 1/4 | 2.181 | 0.500 | 1.218 | 17.513 |
| 26 | QPSK 1/3 | 3.398 | 0.667 | 1.135 | 16.295 |
| 25 | QPSK 2/5 | 4.533 | 0.800 | 1.284 | 15.160 |
| 24 | QPSK 1/2 | 5.818 | 1.000 | 1.519 | 13.876 |
| 23 | QPSK 3/5 | 7.337 | 1.200 | 0.404 | 12.357 |
| 22 | QPSK 2/3 | 7.741 | 1.333 | 0.990 | 11.953 |
| 21 | QPSK 3/4 | 8.731 | 1.500 | 0.601 | 10.963 |
| 20 | QPSK 4/5 | 9.332 | 1.600 | 0.526 | 10.361 |
| 19 | QPSK 5/6 | 9.858 | 1.667 | 1.122 | 9.835 |
| 18 | QPSK 8/9 | 10.981 | 1.778 | 0.245 | 8.713 |
| 17 | QPSK 9/10 | 11.226 | 1.800 | 3.552 | 8.468 |
| 16 | 8PSK 3/5 | 14.777 | 1.800 | 0.706 | 4.916 |
| 15 | 8PSK 2/3 | 15.483 | 2.000 | 1.478 | 4.211 |
| 14 | 8PSK 3/4 | 16.961 | 2.250 | 1.319 | 2.733 |
| 13 | 8PSK 5/6 | 18.280 | 2.500 | 1.196 | 1.414 |
| 12 | 8PSK 8/9 | 19.475 | 2.667 | 0.218 | 0.218 |
| 11 | 8PSK 9/10 | 19.694 | 2.700 | n/a | 0.000 |
| 10 | 16APSK 5/6 | 30.300 | 3.333 | 0.210 | 6.900 |
| 9 | 16APSK 4/5 | 30.510 | 3.200 | 0.005 | 6.690 |
| 8 | 16APSK 9/10 | 30.515 | 3.600 | 0.285 | 6.685 |
| 7 | 16APSK 3/4 | 30.800 | 3.000 | 0.200 | 6.400 |
| 6 | 16APSK 8/9 | 31.000 | 3.556 | 0.200 | 6.200 |
| 5 | 16APSK 2/3 | 31.200 | 2.667 | 5.600 | 6.000 |
| 4 | 32APSK 5/6 | 36.500 | 4.000 | 0.150 | 0.700 |
| 3 | 32APSK 9/10 | 36.650 | 4.500 | 0.050 | 0.550 |
| 2 | 32APSK 8/9 | 36.700 | 4.444 | 0.100 | 0.500 |
| 1 | 32APSK 4/5 | 36.800 | 4.167 | 0.400 | 0.400 |
| 0 | 32APSK 3/4 | 37.200 | 3.750 | n/a | 0.000 |

The difference of the required $E_s/N_0$ at $P_b = 10^{-5}$ between the ACM mode $i$-1 and $i$, except for ACM mode $i = 0$, was computed using the third column of Table 6 and is listed in the fifth column using Eq. (9). This difference was used to find the best ACM mode from the current ACM mode $i$, depending on the attenuation under Rician fading. It is desirable to use an ACM mode of a lower index for a higher BWE, if the received SNR meets the minimum required SNR in Table 6. Refer to the fourth column of Table 6, which lists the BWE $\eta_i$ of each ACM mode $i$. If the received SNR under Rician is between $(E_s/N_0)_{i-1} - (E_s/N_0)_i$ and $(E_s/N_0)_i$, then it used ACM mode $i$ to maximize the BWE because (a) the SNR was not sufficient to use the ACM mode $i$-1 and to achieve $BER \leq 10^{-5}$, but the SNR was sufficient to support ACM mode $i$ and to achieve $BER \leq 10^{-5}$ under Rician, and because (b) an ACM mode with a lower mode index yields a higher BWE, as shown in the fourth column.

The highest ACM mode under AWGN was 32APSK9/10 and required the received SNR to be $E_s/N_0$ = 15.799 dB at $P_b = 10^{-5}$. Hence, the nominal operating received SNR was assumed to be $E_s/N_0$ = 15.799 dB. However, under Rician fading, the required received SNR should be $E_s/N_0$ = 37.200 dB even at $P_b = 10^{-5}$. Therefore, to support the ACM mode 0 (i.e., 32APSK ¾) of the highest BWE under Rician fading, it required additional transmitted power of 37.20 - 15.799 = 21.401 dB.

If the extra link margin, $x_{LM}$, is 21.401 dB, then the highest ACM mode 32APSK 3/4 can be supported with probability $p_0$. The probability $p_0$ can be obtained from the CDF of the attenuation in Figure 9, e.g., $p_0 \approx 0$ at attenuation $X$=0 dB. However, the link margin of 21.401 dB is hard to achieve in practice.

Probability $p_i$ of other ACM mode $i$ can be obtained from Figure 9. Since the LDPC decoding didn't distinguish each code rate clearly for 16APSK and 32APSK and the BER at a much higher SNR, this wouldn't be practical to transmit at higher symbol-energy-to-noise ratio. Therefore, the BWE is calculated only for QPSK and 8PSK. The highest ACM mode $i$ = 0, i.e., 8PSK 9/10, and then the lowest ACM mode is QPSK 1/4.

Three cases {A, B, and C} of different link margin attenuation were investigated; 0 dB, 10 dB, and 28 dB, respectively. Any other link margins parameter can be used by shifting the value. The average BWE of the W/V-band system in bits/s/Hz is given by Eq. (13) and Eq. (14). Table 7 provides the BWE of 8.0407 Gbits/s for Case A under Rician fading whereas Table 8 provides the corresponding BWE of 9.449 Gbits/s for Case A under AWGN where all ACM modes can be applicable.

**Table 7. BWE Results Under Flat Rician Fading with BW = 5 GHz**

| Case | $E[\eta] \times BW$ ($Gbps$) per antenna beam | Highest Probability ACM Mode ($R_c$) |
|---|---|---|
| A | 8.041 | QPSK (9/10) |
| B | 12.561 | 8PSK (9/10) |
| C | 13.434 | 8PSK (9/10) |

**Table 8. BWE Results Under AWGN with BW = 5 GHz**

| Case | $E[\eta] \times BW$ ($Gbps$) per antenna beam | Highest Probability ACM Mode ($R_c$) |
|---|---|---|
| A | 9.449 | 8PSK (5/6) |
| B | 21.371 | 32APSK (9/10) |
| C | 22.379 | 32APSK (9/10) |

In Table 7, the average BWE for each case in (Gbits/s) per antenna beam, the highest probability ACM mode, and $R_c$ are shown. Observe that the higher link margin yields a higher BWE. However, this requires a higher cost, e.g., a higher transmitting power, a larger antenna size, and a lower noise figure, etc. Case A is the worst. Case B is the most reasonable out of two cases for practical application, but the BER wasn't sufficiently large enough to reach $10^{-5}$and it makes no difference in $E_s/N_0$ among the different ACM modes.

*Remarks*: The BWE results in Table 7 were obtained for the DVB-S2 under a memoryless, no Doppler frequency shift, Rician fading channel environment. If the channel is an AWGN with no Rician fading, then the ACM mode $i$ = 0, i.e., 32APSK 9/10 will require the received $E_s/N_0 \geq$ 15.799 dB to achieve BER of $P_b = 10^{-5}$ from BER curves in Figure 18 and other BERs for 16APSK and 32APSK. However, if the channel is under a Rician fading, then the ACM mode $i$ = 0, i.e., 32APSK 9/10 will require much higher received $E_s/N_0 \geq 27.3$ dB to achieve a worse BER of $P_b = 10^{-5}$ from Table 6 and Figure 15. Hence, the transmitted signal power under the Rayleigh fading channel should be at least 12.5 dB higher than that under the AWGN. Furthermore, the BER under the Rician fading is three decades worse than that under the AWGN.

### 3.5 Frequency Selective Rician Fading Channel Model

In the DVB-S2 standard, there are 28 ACM modes. Any of the 28 ACM mode symbols can be transmitted via an OFDM subcarrier symbol. However, OFDM has not been employed yet for satellite communications. This is because the satellite link has been modelled as an AWGN

channel, whereas OFDM is the main modulation in the 5G terrestrial communications. In this section, it is recommended to include an OFDM for future 6G terrestrial communications, especially when an interface link between W/V-band satellite communications and future 6G terrestrial communications is desirable. In addition, OFDM is effective against a frequency selective Rician fading terrestrial channel environment when a high data rate transmission is desirable. In this section, multiple multipath Rician fading is investigated using the DVB-S2 system and OFDM communication systems, and the BWE is calculated where two multipath profiles are generated with seventy and thirty percent of the total received power through the two Rician fading multipaths.

The main difference between Rayleigh and Rician fading channel models is the mean of the in-phase and quadrature-phase component *X* and *Y* of the multipath channel. For Rayleigh fading, the means of *X* and *Y* are zero, i.e., only the NLOS multipaths are available. On the other hand, for Rician fading, the means of *X* and *Y* are nonzero because Rican fading is the sum of a LOS component and multiple NLOS signal components. The average power ratio of the LOS components over that of NLOS in a Rician fading is called by a Rician factor *K*. Both *X* and *Y* are Gaussian random variables, independent, and identical.

Hence, for Rayleigh fading, two Gaussian random variables *X* and *Y* have zero means and equal variance of $\sigma^2$. The amplitude $Z = \sqrt{X^2 + Y^2}$ is called a Rayleigh fading random variable. Therefore, $Z^2 = X^2 + Y^2$ becomes an exponentially distributed random variable. Both random variables *X* and *Y* are simulated by two Gaussian random variables with mean zero and variance $\sigma^2$ as:

$$X = r_I(t) = \sum_{n=0}^{N(t)} \alpha_n(t) cos\emptyset_n(t) \quad \sim N(0, \sigma^2) \tag{20}$$

and

$$Y = r_Q(t) = \sum_{n=0}^{N(t)} \alpha_n(t) sin\emptyset_n(t) \quad \sim N(0, \sigma^2) \tag{21}$$

where $\alpha_n(t)$ and $\emptyset_n(t)$ are, respectively, the amplitude and phase random variables for the *n*-th multipath component, and $\emptyset_n(t)$ is a uniform random variable between 0 and 2π. Then, the Rayleigh random variable is generated as $Z = \sqrt{X^2 + Y^2}$. The Rayleigh random variable probability density function can be written as:

$$p_Z(z) = \frac{2z}{\overline{P_r}} \exp\left[-\frac{z^2}{\overline{P_r}}\right] = \frac{2z}{\sigma^2} \exp\left[-\frac{z^2}{2\sigma^2}\right] \quad , z \geq 0. \tag{22}$$

where $\overline{P_r} = E[Z^2] = E[X^2 + Y^2] = 2\sigma^2$ is the average received total signal power.

On the other hand, for the Rician multiple multipath fading (i.e., frequency selective fading), the channel consists of an LOS path and multiple NLOS paths. The channel of the LOS component is a constant as:

$$r_{I,LOS}(t) = \alpha_0(t) cos\emptyset_0(t)\,, \tag{23}$$

$$r_{Q,LOS}(t) = \alpha_0(t) sin\emptyset_0(t), \tag{24}$$

and the summation of the NLOS components has a Gaussian random variable with a mean of zero and variance of $\sigma^2$. Then, *X* and *Y* are the sum of the LOS and NLOS components, which are defined as:

$$X = \alpha_0(t)cos\emptyset_0(t) + \sum_{n=1}^{N(t)} \alpha_n(t)cos\emptyset_n(t) \sim N(\alpha_0(t)cos\emptyset_0(t), \sigma^2) \quad (25)$$

$$Y = \alpha_0(t)sin\emptyset_0(t) + \sum_{n=1}^{N(t)} \alpha_n(t)sin\emptyset_n(t) \sim N(\alpha_0(t)sin\emptyset_0(t), \sigma^2) \quad (26)$$

where the LOS is a constant and the NLOS is a Gaussian random variable. The expectation and variance of *X* and *Y* can be written, respectively, as:

$$E[X] = \alpha_o(t)cos\emptyset_0(t)(t), \sigma_x^2 = E[(X - \mathrm{E}[X])^2] = \sigma^2 \quad (27)$$

and

$$E[Y] = \alpha_o(t)sin\emptyset_0(t), \ \sigma_y^2 = E[(Y - \mathrm{E}[Y])^2] = \sigma^2. \quad (28)$$

The power of the LOS component is called the non-centrality of the Rician random variable and written as:

$$s^2 = E^2[X] + E^2[Y] = {\alpha_o}^2(t)cos^2\emptyset_0(t) + {\alpha_o}^2(t)sin^2\emptyset_0(t)] = {\alpha_o}^2(t). \quad (29)$$

The Rician fading average received power is written as:

$$\bar{P_r} = E[Z^2] = E[X^2] + E[Y^2] = \sigma^2 + {\alpha_o}^2(t)cos^2\emptyset_0(t) + \sigma^2 + {\alpha_o}^2(t)sin^2\emptyset_0(t) = 2\sigma^2 + {\alpha_o}^2 = 2\sigma^2 + s^2. \quad (30)$$

The probability density function $p_Z(z)$ of the Rician random variable $Z = \sqrt{X^2 + Y^2}$ can be written as:

$$p_Z(z) = \frac{z}{\sigma^2}\exp\left[\frac{-(z^2+s^2)}{2\sigma^2} I_o\left(\frac{zs}{\sigma^2}\right)\right], \ z \geq 0 \quad (31)$$

$$\bar{P_r} = E[Z^2] = \int_0^\infty z^2 \, p_Z(z)dz = 2\sigma^2 + s^2 \quad (32)$$

where $I_o(\cdot)$ is the modified Bessel function of the first kind. Since the Rician *K*-factor is the ratio of the LOS signal power over all the NLOS component signal power, it becomes a Rayleigh fading when *K* = 0, and no fading when *K* = ∞ where:

$$K = \frac{s^2}{2\sigma^2}. \quad (33)$$

The non-centrality parameter $s^2$ (which is equal to the LOS power) and the NLOS component fading power $2\sigma^2$ can be written in terms of the Rician factor *K*, respectively, as:

$$s^2 = \frac{\bar{P_r}\,K}{1+K} \quad (34)$$

and

$$2\sigma^2 = \frac{\bar{P_r}}{1+K}. \quad (35)$$

The corresponding MATLAB source code is shown in the Appendix 4. The Rician factor $K$_dB was set to 12 dB, as shown in line 1, since that value was a practical ratio for an outdoor fading environment. The average received power, Pr_av, was set to 1. Line 3 converts $K$_dB into a linear scale as $K$. Lines 4 and 5 are for values $s$ and $\sigma$, based on Eq. (34) and Eq. (35), respectively. Depending upon the modulation order size, the "modOut" variable in line 13 or 15 of the MATLAB source code represents the modulated symbol after low-density parity-check (LDPC) encoding for a given code rate, and the DVB-S2 specific interleaver structure will need to enter a serial-to-parallel conversion. Depending on the size of the "modOut" column matrix of QPSK, 8PSK, 16APSK, and 32APSK, it would be divided into 1,024 subcarriers to pass through the serial-to-parallel conversion to be processed into the OFDM modulator shown in Figure 10. In this work, the fast Fourier transform of size 1024 was used. In other words, the column matrix of "modOut" becomes a matrix size 1024 by the number of divisible rows of 1024 subcarriers. Since the DVB-S2 frame size is not a multiple of 1024, the final column was padded by zero for the remainder portion. Lines 26-27 in Appendix 4 show the fading coefficient generation.

In Figure 19, Figure 20, Figure 21, and Figure 22, all 28 ACM modes code rates were simulated. Since $10^{-5}$ BER could not be achieved, BERs at $10^{-2}$ were recorded into the BWE calculation and re-ranked. Figure 19, Figure 20, Figure 21, and Figure 22 show BERs of the DVB-S2 ACM modes when the OFDM is used under the two-path frequency-selective multipath Rician fading channel with 0.7 power at the first and 0.3 power at the second path and four-symbol time intervals separation between two path arrival times.

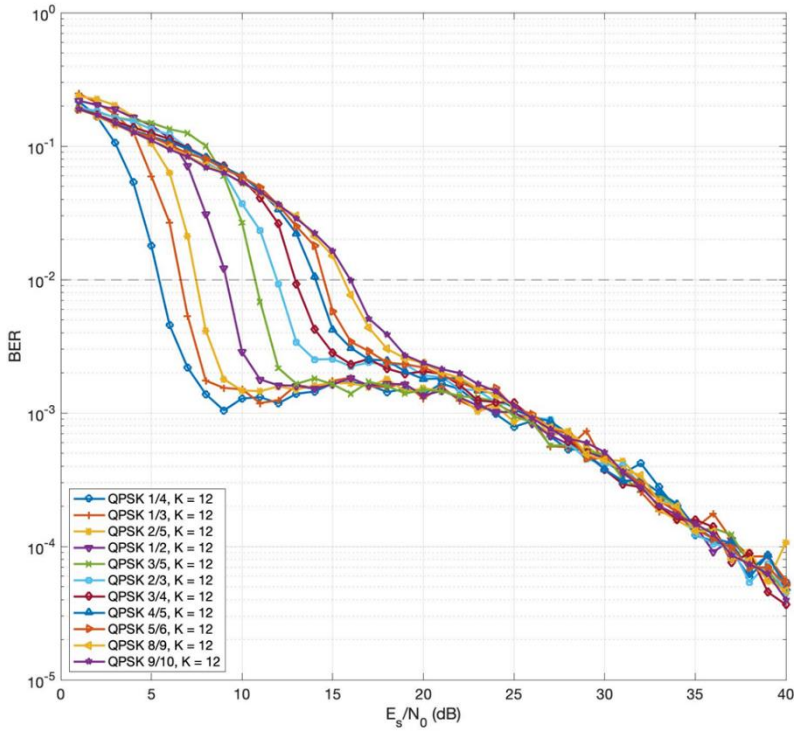


**Figure 19. DVB-S2 QPSK Two Multipath Rician Fading with OFDM**

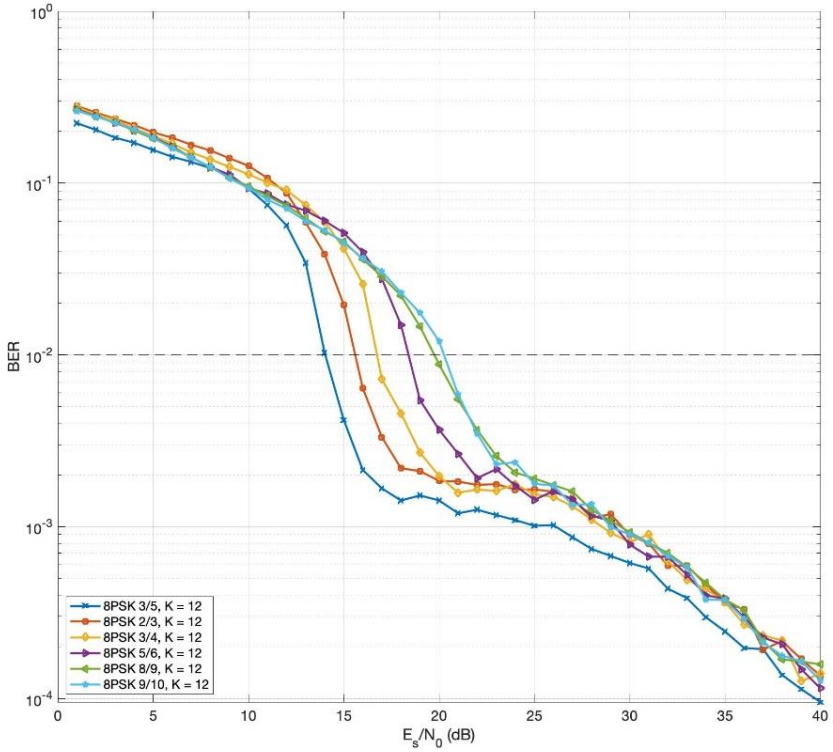


**Figure 20. DVB-S2 8PSK Two Multipath Rician Fading with OFDM**

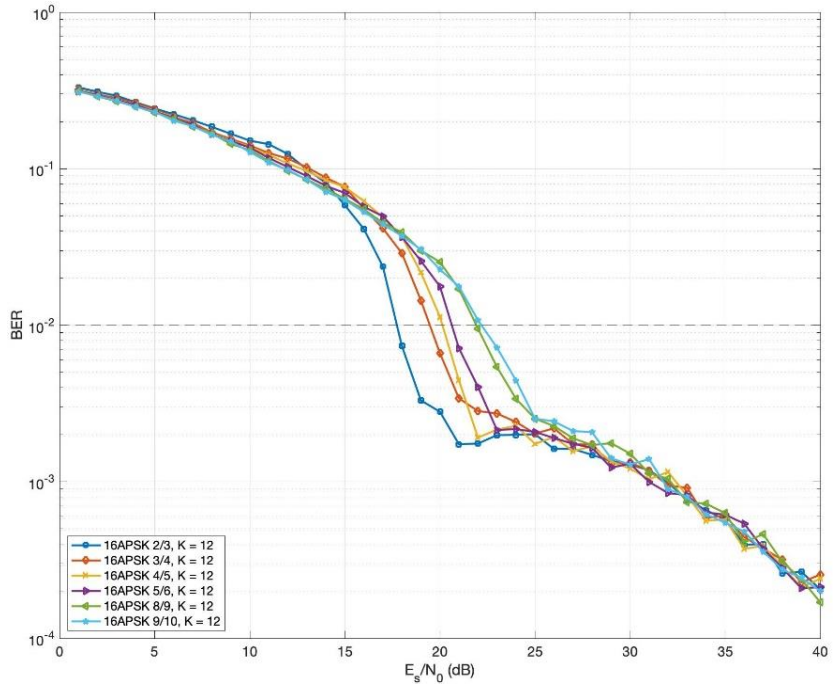


**Figure 21. DVB-S2 16APSK Two Multipath Rician Fading with OFDM**

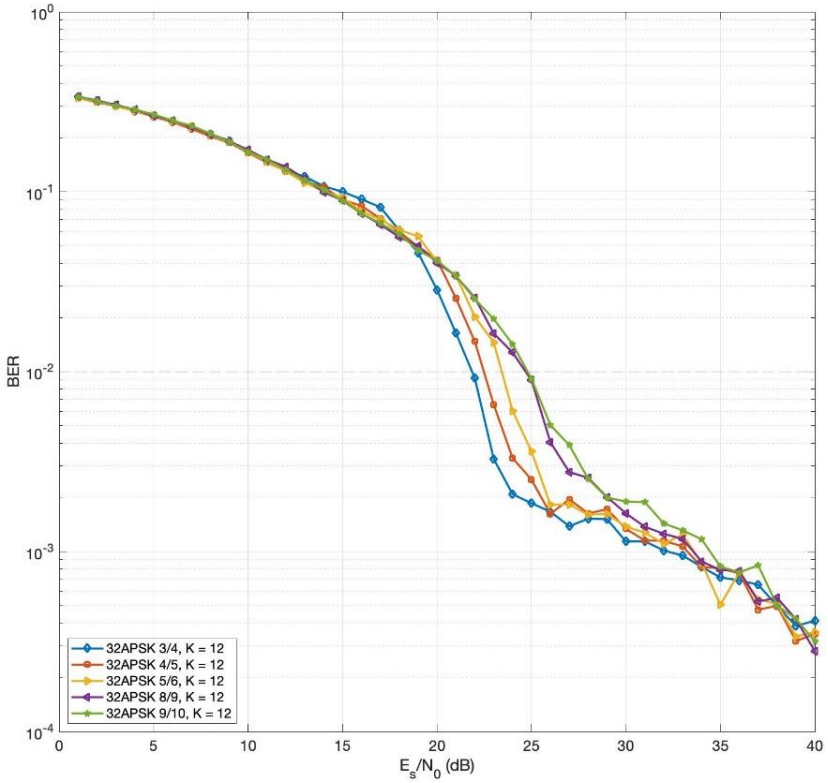


**Figure 22. DVB-S2 32APSK Two Multipath Rician Fading with OFDM**

In Table 9, each ACM mode's code rate is ranked, and the cumulative distribution function (CDF) of the W/V-band attenuation in dB, shown in Figure 9, is applied with a link margin of 0 dB for Case A. In Table 10, the BWE is listed since it has the highest BWE, and the 7.199 Gbps rate can be supported per antenna beam with an ACM mode of QPSK 9/10 and link margin 8.828 dB. It was reported in the previous section that the highest BWE under a two multipath Rayleigh fading with OFDM at link margin 16.36 dB was 6.62 Gbps with QPSK (1/2).

**Table 9. BWE Results Under Two Multipath Rician Fading Channel of Rician Factor $K$ = 12 dB with OFDM and BW=5 GHz**

| Mode Index $i$ | ACM Mode $i$ | Required $(E_s/N_0)_i$ $dB$ at $P_b = 10^{-2}$ | $\eta_i = R_c log_2 M(i)$ $\left(\frac{bps}{Hz}\right)$ | $\Delta(E_s/N_0)_i = (E_s/N_0)_{i-1} - (E_s/N_0)_i$ $dB$ | $x_i = (E_s/N_0)_0 - (E_s/N_0)_i$ $dB$ |
|---|---|---|---|---|---|
| 27 | QPSK 1/4 | 5.425 | 0.500 | 1.185 | 19.371 |
| 26 | QPSK 1/3 | 6.610 | 0.667 | 0.850 | 18.186 |
| 25 | QPSK 2/5 | 7.460 | 0.800 | 1.675 | 17.336 |
| 24 | QPSK 1/2 | 9.135 | 1.000 | 1.585 | 15.661 |
| 23 | QPSK 3/5 | 10.720 | 1.200 | 1.199 | 14.076 |
| 22 | QPSK 2/3 | 11.919 | 1.333 | 1.009 | 12.877 |
| 21 | QPSK 3/4 | 12.928 | 1.500 | 1.125 | 11.868 |
| 18 | 8PSK 3/5 | 14.028 | 1.800 | 1.574 | 10.768 |
| 20 | QPSK 4/5 | 14.053 | 1.600 | 0.462 | 10.743 |
| 19 | QPSK 5/6 | 14.515 | 1.667 | -0.487 | 10.281 |
| 15 | 8PSK 2/3 | 15.600 | 2.000 | 1.144 | 9.196 |
| 17 | QPSK 8/9 | 15.602 | 1.778 | 0.366 | 9.194 |
| 16 | QPSK 9/10 | 15.968 | 1.800 | -0.368 | 8.828 |
| 14 | 8PSK 3/4 | 16.744 | 2.250 | 0.994 | 8.052 |
| 13 | 16APSK 2/3 | 17.738 | 2.667 | 0.660 | 7.058 |
| 12 | 8PSK 5/6 | 18.398 | 2.500 | 1.072 | 6.398 |
| 11 | 16APSK 3/4 | 19.470 | 3.000 | 0.279 | 5.326 |
| 10 | 8PSK 8/9 | 19.749 | 2.667 | 0.507 | 5.047 |
| 8 | 16APSK 4/5 | 20.133 | 3.200 | 0.495 | 4.663 |
| 9 | 8PSK 9/10 | 20.256 | 2.700 | -0.123 | 4.540 |
| 7 | 16APSK 5/6 | 20.628 | 3.333 | 1.227 | 4.168 |
| 6 | 32APSK 3/4 | 21.855 | 3.750 | 0.062 | 2.941 |
| 5 | 16APSK 8/9 | 21.917 | 3.556 | 0.267 | 2.879 |
| 4 | 16APSK 9/10 | 22.184 | 3.600 | 0.294 | 2.612 |
| 3 | 32APSK 4/5 | 22.478 | 4.000 | 0.948 | 2.318 |
| 2 | 32APSK 5/6 | 23.426 | 4.167 | 1.264 | 1.370 |
| 1 | 32APSK 8/9 | 24.690 | 4.444 | 0.106 | 0.106 |
| 0 | 32APSK 9/10 | 24.796 | 4.500 | n/a | 0.000 |

**Table 10. Required $E_s/N_0$ at $P_b = 10^{-2}$ and BWE Under Two Multipath Rician Fading with OFDM and Link Margin of 8.828 dB**

| Case | $E[\eta] \times BW$ $(Gbps)$ per Antenna Beam | Highest Probability ACM Mode ($R_c$) |
|---|---|---|
| A | 7.199 | QPSK (9/10) |

### 3.6 5G Polar FEC and Flat Rayleigh Fading

In the previous sections, DVB-S2 protocol was simulated under different fading conditions to investigate the bandwidth efficiency of a W/V-band channel using the LDPC error-correction code and ACM specified in the DVB-S2 standard. It was reported that most of the ACM modes could not reach the desirable bit error rate (BER) of $P_b = 10^{-5}$ for 8-ary phase-shift keying (8PSK), 16-ary amplitude phase-shift keying (16APSK), and 32-ary amplitude phase-shift keying (32APSK) under a flat (i.e., single multipath) or a frequency-selective (i.e., multiple multipath) Rayleigh or Rician fading channel environment. This observation was the motivation for investigating the polar forward error-correction code (FEC) as a replacement for the LDPC coding and to explore any significant improvements under terrestrial fading channels. Typical satellite communication systems like the DVB-S2 system have been built assuming an AWGN channel model. Recently, a new trend has emerged to connect the 5G terrestrial communication systems to satellite communication systems. Therefore, it is desirable to investigate and design a new W/V-band communication system under both satellite and terrestrial communication system environments.

The polar error correction code was introduced by Erdal Arikan in July 2009 and constructed on the idea of channel polarization [16]. It has been used in the 5G-Third Generation Partnership Project (3GPP) standard along with LDPC coding to assist in improving the channel capacity, i.e., maximum achievable data rate with an arbitrary small BER. In this work, the polar error-correction code and the ACM in the 5G standard, such as quadrature phase-shift keying (QPSK), 16-ary quadrature amplitude modulation (16QAM), 64-ary quadrature amplitude modulation 64QAM, and 256-ary quadrature amplitude modulation 256QAM, are simulated.

For a polar error-correction codeword generation (i.e., encoding), a Kronecker product is computed recursively starting with a 2 × 2 kernel. The generator matrix, $G_N$, has a size of $N = 2^n$, where $n$ denotes the level and can be any integer greater than or equal to 1, such that the matrix size is $N \times N$. For example,

$$G_2 = \begin{bmatrix} 1 & 0 \\ 1 & 1 \end{bmatrix} \text{ (kernel).} \tag{36}$$

The polar encoder takes the incoming message sequence, $u_i$, breaks it into a pair of two-bit lengths, and generates the output of two bits when $N = 2$. For a $G_2$ polar transform, two input bits are converted into two output bits for the level-2 output ($u^{(2)}$) as:

Input → Output

$$[u_1, u_2]G_2 \rightarrow [u_1 + u_2\,, u_2] \tag{37}$$

where + denotes the modulo-2 additions shown in Table 11.

**Table 11. List of Modulo-2 Additions**

| Input ($u_i$) | | Output ($u^{(2)}$) |
|---|---|---|
| $u_1$ | $u_2$ | |
| 0 | 0 | 0 0 |
| 0 | 1 | 1 1 |
| 1 | 0 | 1 0 |
| 1 | 1 | 0 1 |

In Figure 23, the graph is presented of a binary tree representation for level 2 output bits: $u^{(2)} = [u_1 + u_2\,, u_2]$, which converts 2 input bits to 2 output bits. The tree node, $u^{(2)}$, represents two output bits at depth level 0, and the leaf nodes $(u_1, u_2)$ represent 1 input bit each for a total of 2 bits where the depth level is 1.

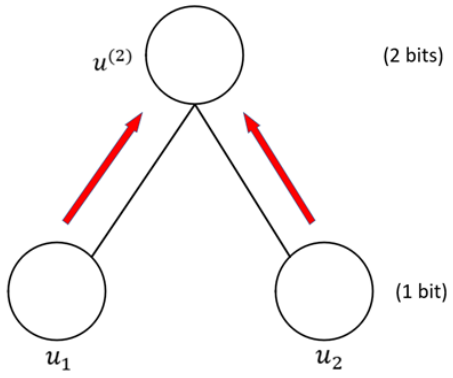


**Figure 23. Binary Tree Representation for Level 2 Output Bits**

To expand the polar transform into 4 bits, the generating matrix, $G_4$, is constructed by taking the Kronecker product of $G_2 \otimes G_2$ as:

$$G_4 = G_2 \otimes G_2 = \begin{bmatrix} 1 & 0 \\ 1 & 1 \end{bmatrix} \otimes \begin{bmatrix} 1 & 0 \\ 1 & 1 \end{bmatrix} = \begin{bmatrix} 1 & 0 & 0 & 0 \\ 1 & 1 & 0 & 0 \\ 1 & 0 & 1 & 0 \\ 1 & 1 & 1 & 1 \end{bmatrix} \text{(kernel)}. \tag{38}$$

Then, 4 input bits are multiplied by the kernel, $G_4$, to get four output bits as:

Input → Output

$$[u_1, u_2, u_3, u_4]G_4 \rightarrow [u_1 + u_2 + u_3 + u_4\,, u_2 + u_4\,, u_3 + u_4\,, u_4 = [u_1^{(2)} + u_2^{(2)}, u_2^{(2)}]. \quad (39)$$

The output bits in Eq. (39) have similar properties as Eq. (37), and a recursion expression will be used where the depth level $d$ increases towards the leaf nodes by 1. An example depth level is shown on the left side of the binary tree representation in Figure 24.

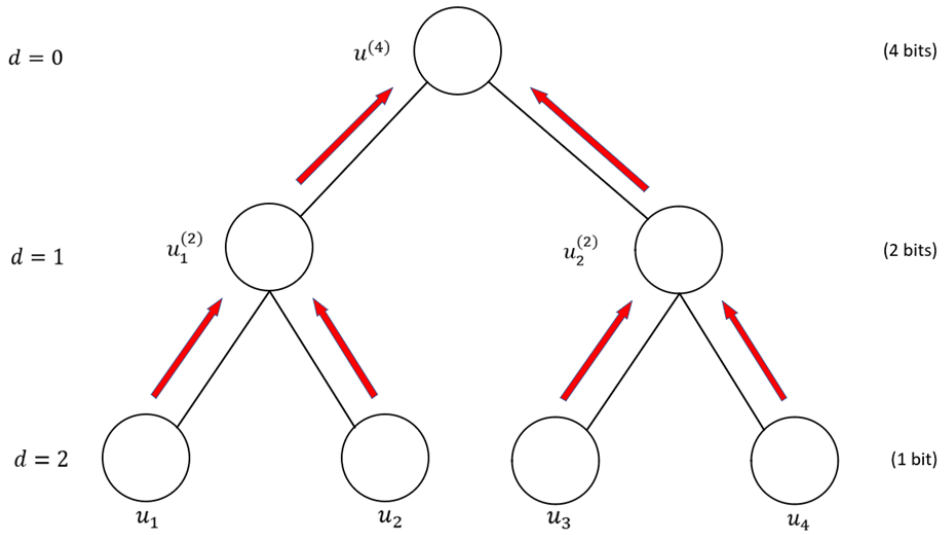


**Figure 24. Binary Tree Representation for Level 4 Output Bits**

The reliability sequence sets the order in which the message bits are rearranged in the leaves, i.e., bottom level in the binary tree representation. Suppose that a message vector $\boldsymbol{u}$ of length $N = 2^n$ bits wants to be formed. However, the actual message length, $K$, can be less than or equal to the polar code word length $N$ (i.e., $K \leq N$). Then, $N$ - $K$ bits must be set to zero for $N - K$ input bits $u_i$ in the bottom level. These input bits are called frozen bits. The number of frozen bits is related to the effective code rate, which is constrained by the channel bandwidth.

For example, consider $N = 8$ and $K = 4$ and suppose that the reliability sequence is set to {1, 2, 3, 5, 4, 6, 7, 8} as recommended by practical experiments. Then, the frozen channels are the first four channels of the reliability sequence, i.e., {1, 2, 3, 5}. Then, the last four channel bits $u_i$ {4, 6, 7, 8} in the reliability sequence are set to the $K = 4$ message bits. In Figure 25, the message bits and frozen bits are assigned, based on the reliability sequence, then encoded to 8 bits. In the 5G 3GPP standard, $N$ is set to 1024 bits and $K$ is a variable depending on the code rate necessary.

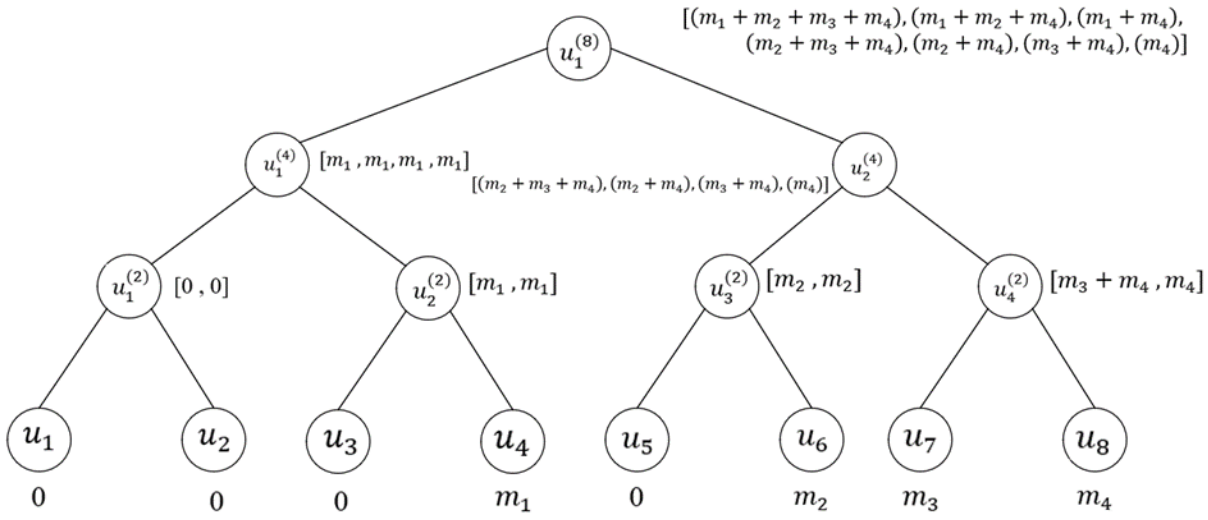


**Figure 25. Assigned Message Bits and Frozen Bits**

In the basic building block of an iterative error-correction decoder with $N = 2$, the $u_1$ should be decoded first. In Figure 26, $r_1$ and $r_2$ are the two received bits, and these are the "beliefs" for $x_1$ and $x_2$, respectively. The likelihood of $u_1$ is a function of $r_1$ and $r_2$ in Eq. (40), which is the min-sum algorithm. The belief for $u_1$ is given as:

$$L(u_1) = f(r_1, r_2) = sign(r_1)\, sign(r_2) \min(|r_1|, |r_2|) \tag{40}$$

$$\hat{u}_1 = 0, if\ L(u_1) \geq 0$$
$$\hat{u}_1 = 1, if\ L(u_1) < 0$$

Here, $sign(r_i)$ denotes the sign of $r_i$, and min $(|r_1|, |r_2|)$ is the minimum of $|r_1|$ and $|r_2|$. Given $\hat{u}_1$, then decode $u_2$ as a function of $r_1$, $r_2$, and $\hat{u}_1$, to determine the likelihood of $u_2$

$$L(u_2) = g(r_1, r_2, \hat{u}_1) = r_2 + (1 - 2\hat{u}_1) r_1 \tag{41}$$

If $\hat{u}_1 = 0$, then $L(u_2) = r_2 + r_1$ $(x = [u_2, u_2])$

If $\hat{u}_1 = 1$, then $L(u_2) = r_2 - r_1$ $(x = [\bar{u}_2, u_2])$

where $\bar{u}_2$ denotes the complement of $u_2$. Figure 27 shows the basic building block of how the message is passed on the tree.

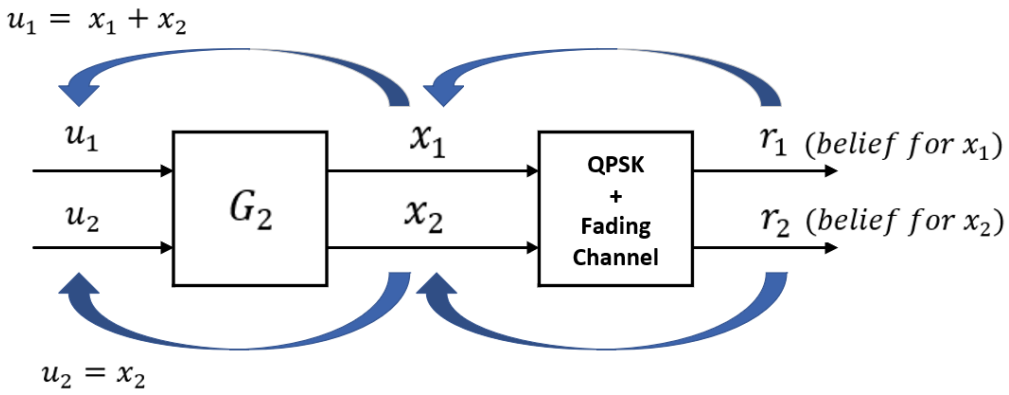


**Figure 26. Two Received Bits $r_1$ and $r_2$ That are Beliefs for $x_1$ and $x_2$**

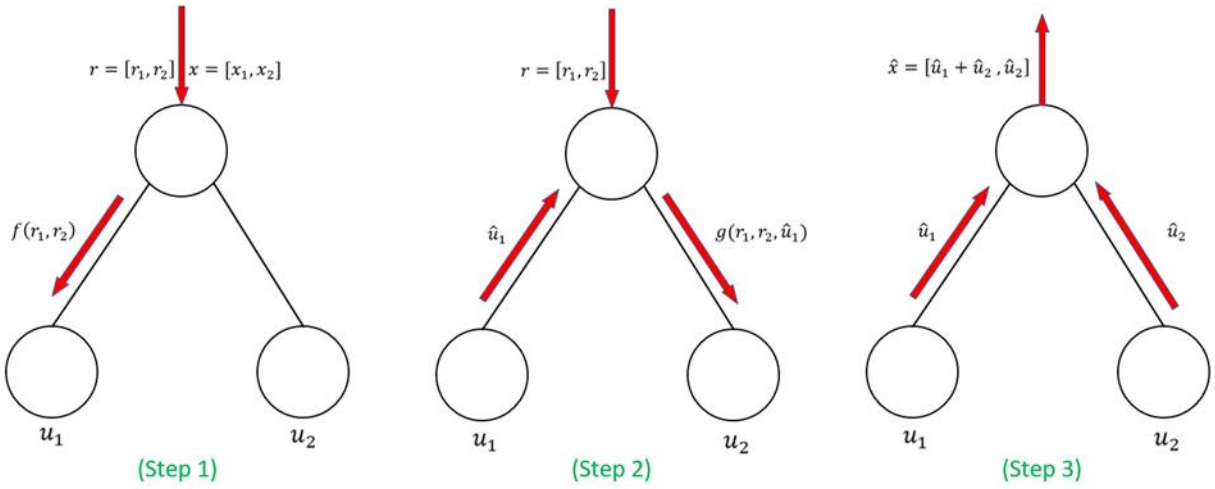


**Figure 27. Basic Building Block of How the Message is Passed on the Tree**

The same channel models such as AWGN, a single multipath (i.e., flat) Rayleigh fading, and a multiple multipath Rayleigh fading, were used in this model and simulation. Additionally, OFDM was used. Further, the 5G terrestrial communication system MATLAB simulator was used instead of the DVB-S2 satellite communication protocol. The previous DVB-S2 simulation results were used to compare with those of the 5G polar error-correction code plus QPSK modulation with code rate 1/2. The signal constellation of QPSK in the DVB-S2 system was the same as that of the 4QAM in the 5G system. So, either QPSK or 4QAM was used. Figure 28 shows a general block diagram of the 5G transmitter and receiver used for this simulation.

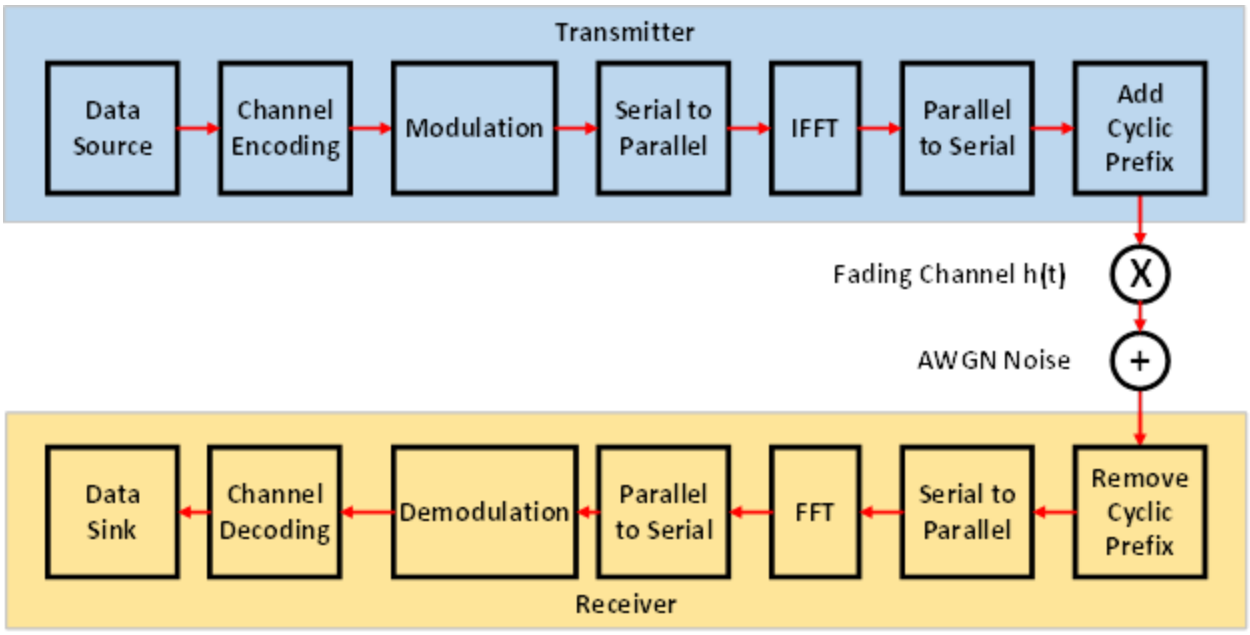


**Figure 28. A General Block Diagram of the 5G Transmitter and Receiver**

The number of message bits, *K*, were randomly generated for simulation and the codeword length *N* was set to *E* for each iteration. The *E* value can be smaller than *N*, and hence the actual code rate in terms of the ratio of the number of message bits over the number of transmitted coded bits can be written as *K*/*E* instead of *K*/*N*.

Simulations were performed for the downlink (DL) from a base station (BS) (or a satellite) to user equipment (UE) (or a ground terminal). MATLAB source code is included in Appendix 5. For example, lines 2 and 3 show the parameters for *K* and *E* as 54 and 124, respectively. The "numFrames" are set to 30,000. It is necessary to have the number of message bits transmitted larger than 100/BER for achieving a reliable simulation BER. Hence, if the BER = $10^{-5}$, then more than $10^{7}$ message bits must be transmitted. The MATLAB 5G toolbox has built-in polar code functions, where the encoding and decoding use these parameters to adjust the size of the reliability sequence based on the codeword vector length $N = E$ and the message length *K*. Then, the message is polar-encoded by using the "nrPolarEncode" function in line 47 before QPSK modulation. The QPSK modulation output symbol is denoted by "modOut" in line 52.

The different fading channels were included in the MATLAB source code:

- Line 54 is for only the AWGN fading channel
- Lines 55–58 are for a single multipath path (i.e., flat) Rayleigh fading
- Lines 61–71 are for a multiple multipath (i.e., frequency-selective fading) Rayleigh fading channel with OFDM.

After the "modOut" symbol was transmitted through the AWGN-plus-Rayleigh fading channel, the received QPSK symbol was demodulated into two bits using a hard-decision and then fed into the "nrPolarDecode" function in the 5G toolbox. Then, the decoder output symbol sequence $\hat{u}_i$ was compared with the transmitted message bit sequence $u_i$ to determine the BER as written in lines 80 and 81. Finally, the measured BER versus the symbol energy-to-noise power-spectral-density *Es*/*N*0 is plotted. The MATLAB toolbox uses SNR instead of $E_s/N_0$. The relation between SNR and Es/No is written as:

$$SNR = R_c\, E_s/N_0 = K/E \times E_s/N_0, \tag{42}$$

where $R_c$ is the actual polar code rate equal to $K/E$. Results are presented in Section 4.1.

### 3.7 Double Layer Encryption

The Department of Defense (DoD) has recently adopted the 5G terrestrial wireless communication service for military communications because the 5G terrestrial communication system can provide a low-latency of one-millisecond and a high-data rate of 800 megabits per second. However, the 5G system is vulnerable under the eavesdropping presence in the wireless medium between a user-equipment (UE) and a terrestrial base station (BS).

The motivation for this investigation is to secure the wireless communication link against an eavesdropping by applying double-layer (i.e., application-layer and physical-layer) encryption in addition to the existing encryption between a UE and a terrestrial BS. Bit streams are encrypted before a channel encoder and decrypted after a channel decoder. Typically, an encryption key output bit stream is added to the bit stream in the application-layer whereas the extra encryption-key output bit stream is added to the data bit stream in the physical-layer that would be done by software or hardware such as a subscriber identity module (SIM) card and integrated circuits (IC) component. Polar code and LDPC code are used as forward error correction codes in the investigation because the 5G employs both polar and LDPC FECs. The encoding structure for polar FEC is from the 5G standard. However, the encoding structure of the LDPC is from the existing standard of the digital video broadcasting-generation 2 satellite (DVB-S2) communications protocol.

Figure 29 presents a flow diagram between a legitimate transmitter (TX) denoted as "Alice" and a legitimate receiver (RX) denoted as "Bob". An unintended receiver is denoted as "Eve" who wants to intercept and decipher the transmission. Alice creates the data block and then adds an encryption key stream to the data block. In this work, both a long key of *l*=512 bits and a short key of *l*=4 bits are considered. The data frame length in the 5G standard is 512 bits long before a channel encoder. The addition of the encryption key stream and data block is done in a bit-by-bit manner with modulo 2-addition. The data-source bit-stream is input to the channel encoder. The encrypted signal from Alice can be expressed as:

$$x_{encrypt,Alice}(n) = x_{data,Alice}(n) \oplus k_{Alice}(n). \tag{43}$$

The decrypted signal at Bob and Eve can be expressed as:

$$y_{decrypt,Bob}(n) = y_{data,Bob}(n) \oplus k_{Bob}(n) = y_{data,Bob}(n) \oplus k_{Alice}(n) \tag{44}$$

$$y_{decrypt,Eve}(n) = y_{data,Eve}(n) \oplus k_{Eve}(n) \tag{45}$$

where $n$ is the bit-time index, and $\oplus$ indicates modulo-2 addition. Encryption / decryption keys are denoted as $k(n)$. The key bit stream at Alice is generated uniformly for a given key-length $l$, and the generated key bit stream is shared with Bob apriori such that

$$k_{Alice}(n) = k_{Bob}(n). \tag{46}$$

The probability that Eve's attempt at the key can be expressed as:

$$Pr[k_{Eve} = k_{Alice}] = \frac{1}{2^l} \tag{47}$$

where $l$ is the key-length.

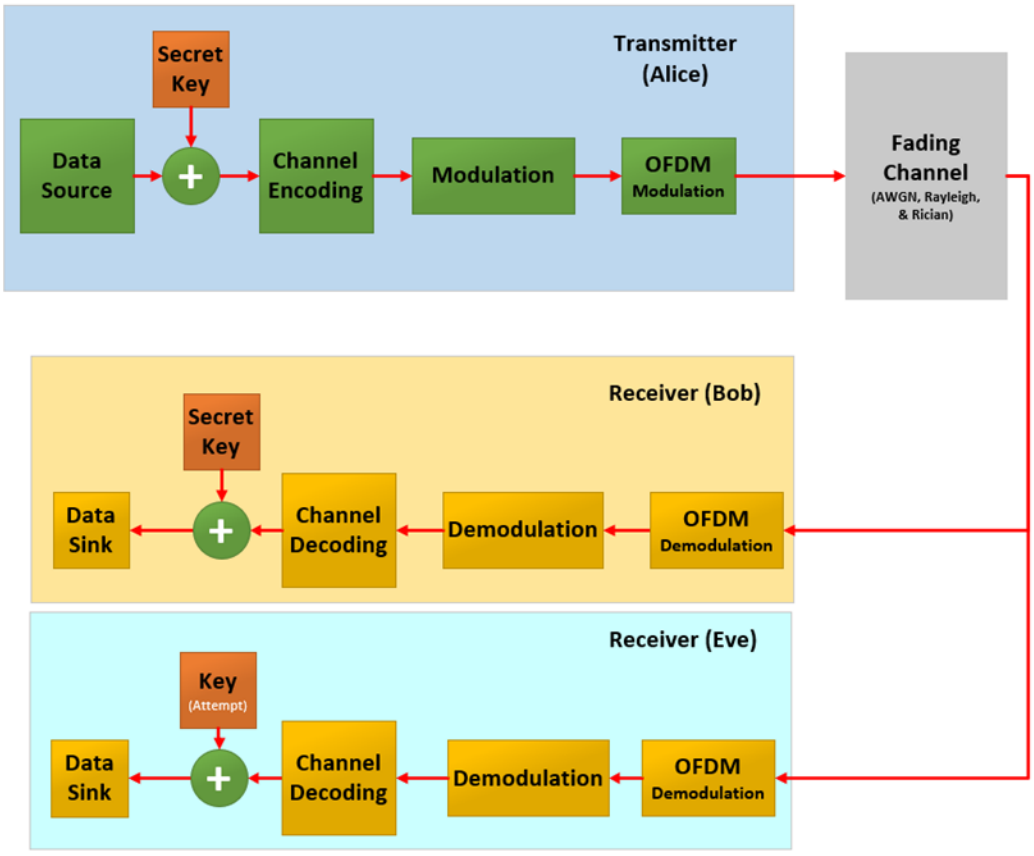


**Figure 29. A Flow Diagram Between Alice, Bob, and Eve**

Alice's encrypted data block undergoes a channel encoding (such as LDPC or polar code). The channel coding rate is set to 1/2. This means that the length of a codeword is 1024 bits long when

an input data block length is 512 bits long. The signal is then modulated. In this analysis, the quadrature-phase-shift-keying (QPSK) modulation is considered which maps every two coded bits into one QPSK modulation symbol. The orthogonal frequency division multiplexing (OFDM) is applied as presented and discussed in previous sections. The modulated symbols are transmitted through additive white Gaussian noise (AWGN), Rayleigh fading, and Rician fading channels.

The same structure used in the previous subsection is employed for channel encoding, modulation, OFDM modulation, fading channels, OFDM demodulation, demodulation, and channel decoding. For example, an OFDM symbol consists of 1024 subcarrier symbols, and multipath 1 and 2 have seventy and thirty percentiles of the total fading channel power equal to 1, respectively. The normalized propagation delays of multipath 1 and 2 are used as time-sample 1 and -sample 4, respectively. One OFDM symbol consists of 1024 time-samples, which carry 1024 subcarrier data, i.e., 1024 coded symbols. A block fading is considered; in other words, the fading channel coefficients are generated every OFDM symbol period and set to be constant.

Bob and Eve then demodulate the received signal, where Bob has the same decryption key as Alice. Eve would attempt to figure out the key and decrypt the message with an incorrect key. Matlab source code for this model and simulation is provided in Appendix 6. Results are provided in section 4.2.

# 4 RESULTS AND DISCUSSION

## 4.1 5G Polar FEC and Flat Rayleigh Fading

Figure 30 shows the BER versus $E_s/N_0$ for both the polar code in the 5G system and the LDPC code in the DVB-S2 system under the AWGN channel, where QPSK modulated symbols were transmitted with code rate $R_c = 1/2$. It is observed that the polar code performed 4.5 dB worse in $E_s/N_0$ than the LDPC coding at $10^{-5}$ BER. This is because of the short codeword length (i.e., 1024 bits) in the polar code whereas the LDPC code word length was 64,800 bits.

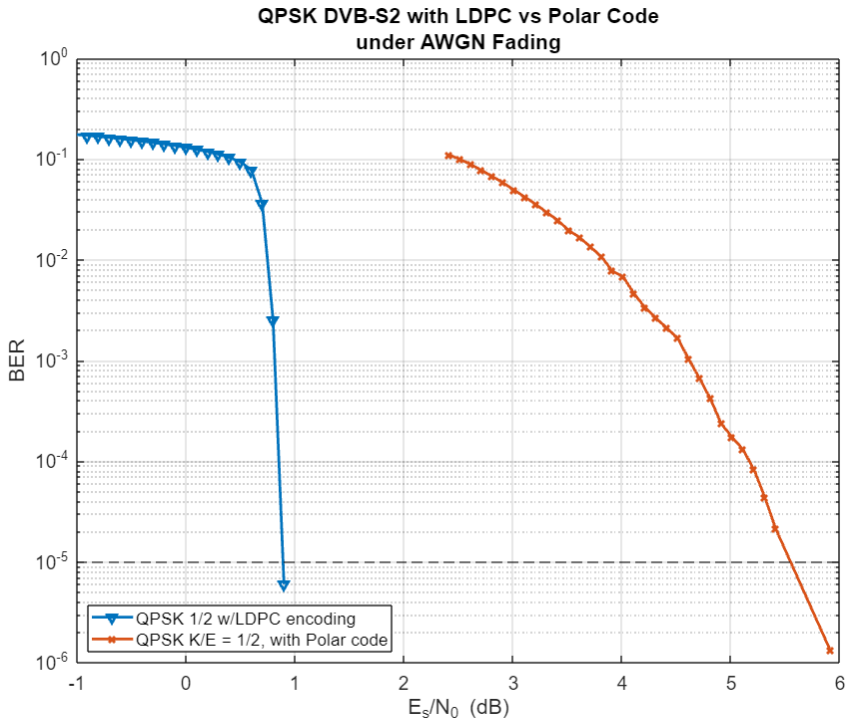


**Figure 30. BER versus $E_s/N_0$ For Both Polar Code and LDPC Code Under AWGN Channel**

Figure 31 shows the BER versus $E_s/N_0$ corresponding to the single multipath (i.e., flat) Rayleigh fading with OFDM. It is observed that the polar code achieved a BER of $10^{-5}$ and performed better than the LDPC coding under the flat Rayleigh fading channel (i.e., ~14 dB better at $P_b = 10^{-3}$).

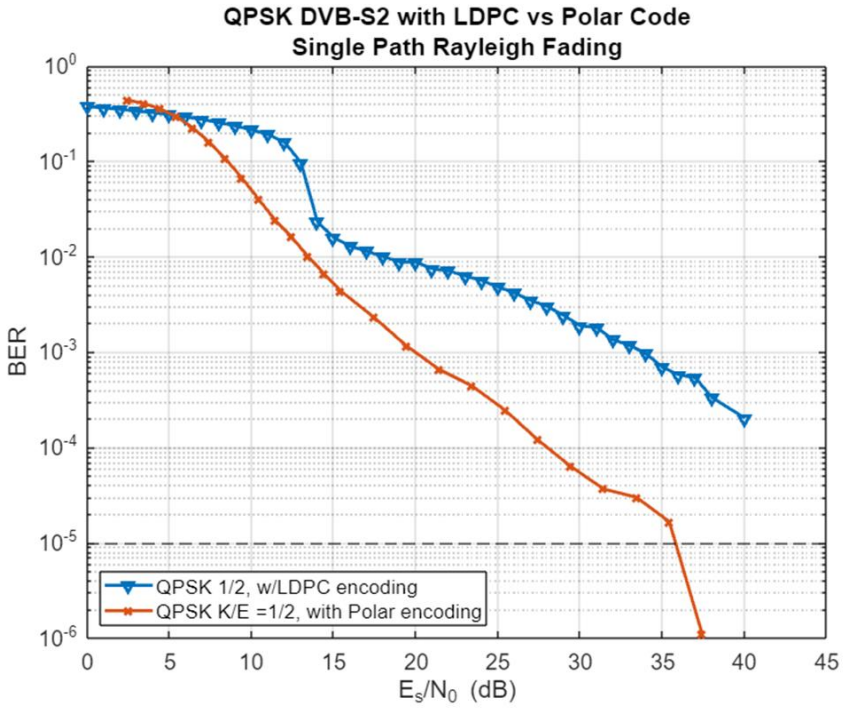


**Figure 31. BER versus $E_s/N_0$ For Both Polar Code and LDPC Code Under Flat Rayleigh Fading Channel**

Figure 32 shows the BER versus $E_s/N_0$ corresponding to two-multiple multipath (i.e., frequency-selective) Rayleigh fading with OFDM. The first and second multipath power was distributed by 70% and 30% of the total channel power equal to 1, respectively. It was observed that the polar code achieved $P_b = 10^{-5}$ BER and performed better than LDPC after $E_s/N_0 = 23$ dB under the frequency selective Rayleigh fading.

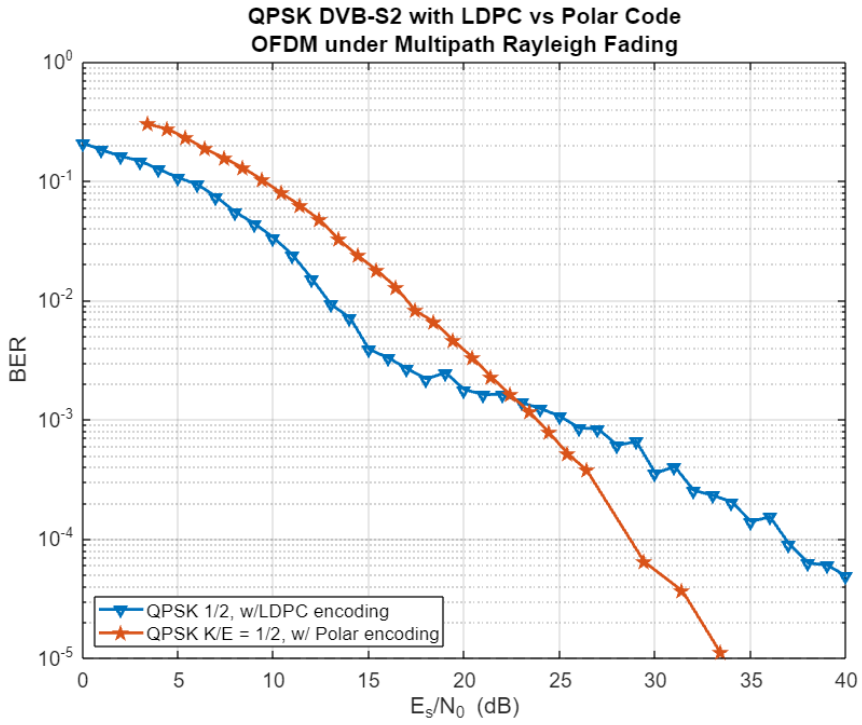


**Figure 32. BER versus $E_s/N_0$ For Both Polar Code and LDPC Code Under Frequency Selective Rayleigh Fading Channel**

## 4.2 Double Layer Encryption

Figure 33 shows the BER versus signal-to-noise ratio (SNR) under AWGN channel with and without encryption. Here, the signal symbol energy was calculated for a coded symbol period. It is observed that the DVB-S2 LDPC code shows 1.5 dB better in SNR at BER equal to $10^{-5}$ than the 5G polar code for both cases with and without encryption. This is because the code word length of DVB-S2 LDPC code is 62,800 symbols which is much longer than 1024 symbols of the 5G polar code. Also, it is observed that the polar code with encryption shows the same BER performance as the case without encryption.

Even if the encryption key length is as short as 4 bits-long, no degradation in BER was observed. This implies that the additional complexity to employ the encryption and decryption is negligible because of the same quality of BER. In addition, the additional delay caused by encryption and decryption for the 5G network is also negligible because only modulo-2 addition is required, which can be implemented with negligible delay.

On the other hand, the BER at Eve is close to 50 percentiles ($P_b = 0.5$) for any SNR, meaning that Eve is not able to achieve the high quality BER of $10^{-5}$ and hence Eve is not able to decrypt the message using the received signal from Alice. This is because Eve is using an attempted key which is not likely to be valid.

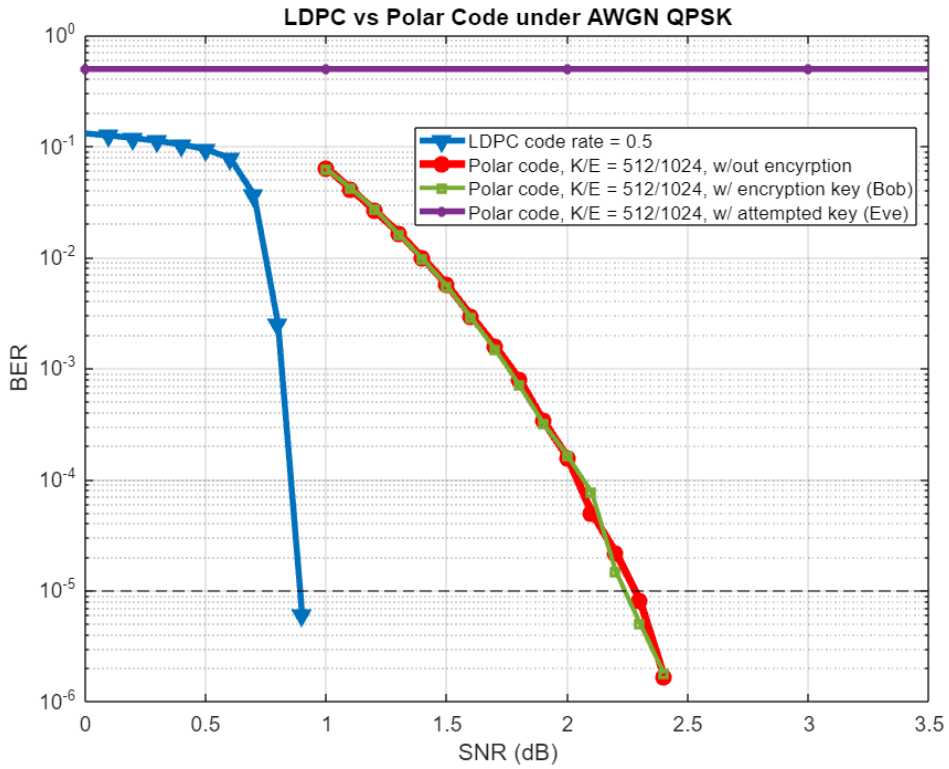


**Figure 33. BER Under AWGN Channel With and Without Encryption**

Figure 34 shows the corresponding BER versus SNR equal to symbol-energy-to-noise-power-spectral-density ratio ($E_s/N_0$) in dB under a single-path Rayleigh fading. The 5G polar code performed better than the DVB-S2 LDPC forward error correction code, even though its code word length was much shorter.

Short and long encryption keys were simulated, and the BER was compared against the message without the encryption key. The same BER performance was observed regardless of key length.

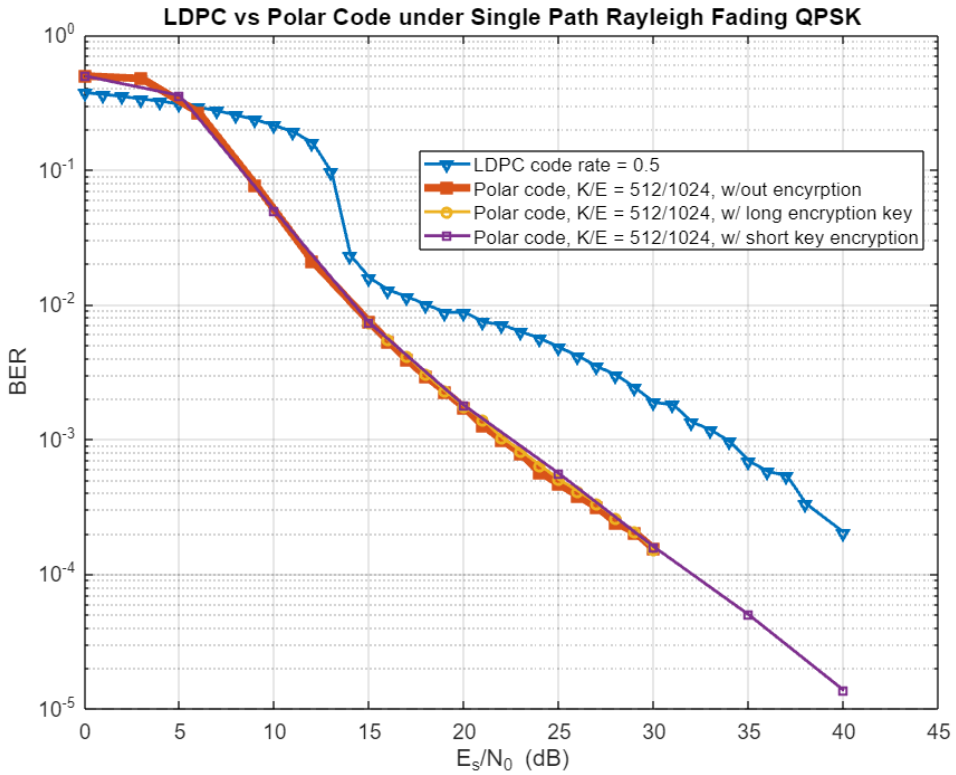


**Figure 34. BER versus SNR Under a Single Multipath Rayleigh Fading**

Figure 35 shows the corresponding BER versus $E_s/N_0$ in dB under two-multipath Rayleigh fading. Multipath 1 and 2 have seventy and thirty percentiles of the total fading channel power, respectively. The normalized propagation delays of multipath 1 and 2 were 1 sample period and 4 sample periods, respectively.

It is observed that the 5G polar code performed worse than the DVB-S2 LDPC FEC code under two-multipath Rayleigh fading. For high SNR (e.g., $E_s/N_o \geq 35$ dB), the 5G polar code performed similarly to the DVB-S2 LDPC FEC code.

Again, short and long encryption keys were also compared. The same BER performance was observed regardless of key-length.

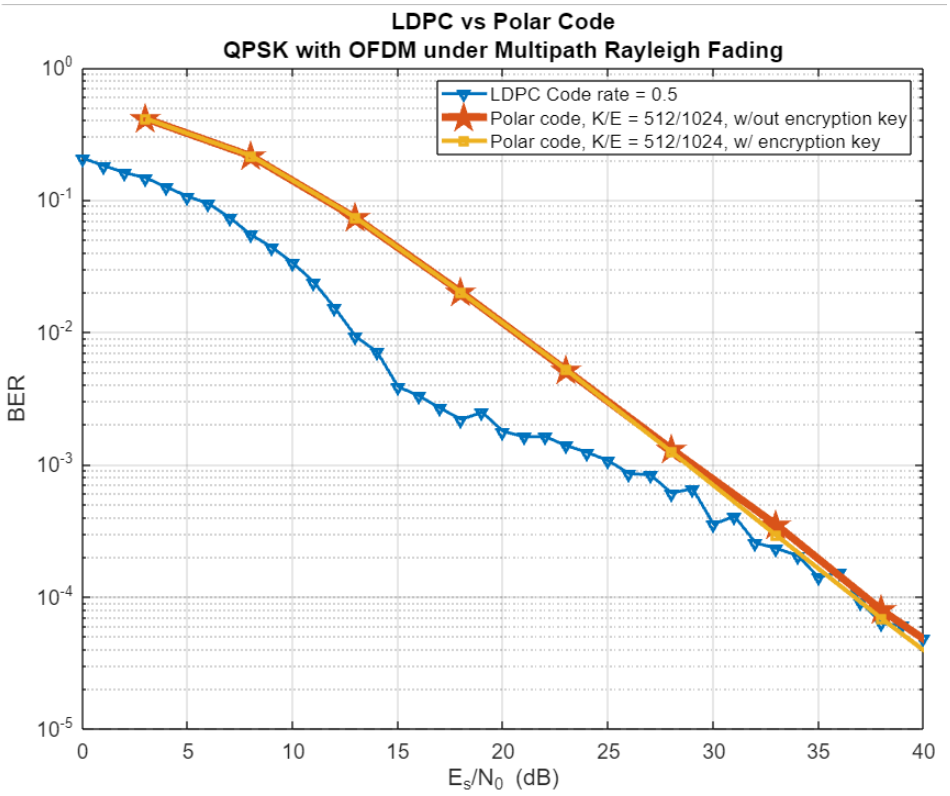


**Figure 35. BER versus SNR Under Two Multipath Rayleigh Fading**

Figure 36 shows the corresponding BER versus $E_s/N_o$ under two-multipath Rician fading with Rician factor $K$ = 12 dB. Multipath 1 and 2 have seventy and thirty percentiles of the total fading channel power, respectively. The normalized propagation delays of multipath 1 and 2 are set to 1 sample period and 4 sample periods, respectively.

For high SNR (e.g., $E_s/N_o \geq 10$ dB), the 5G polar code performed worse than the DVB-S2 LDPC FEC code under two-multipath Rician fading.

Again, short and long encryption keys were tested for the polar code. The BER was compared to the message without encryption. The same BER performance was observed regardless of key length.

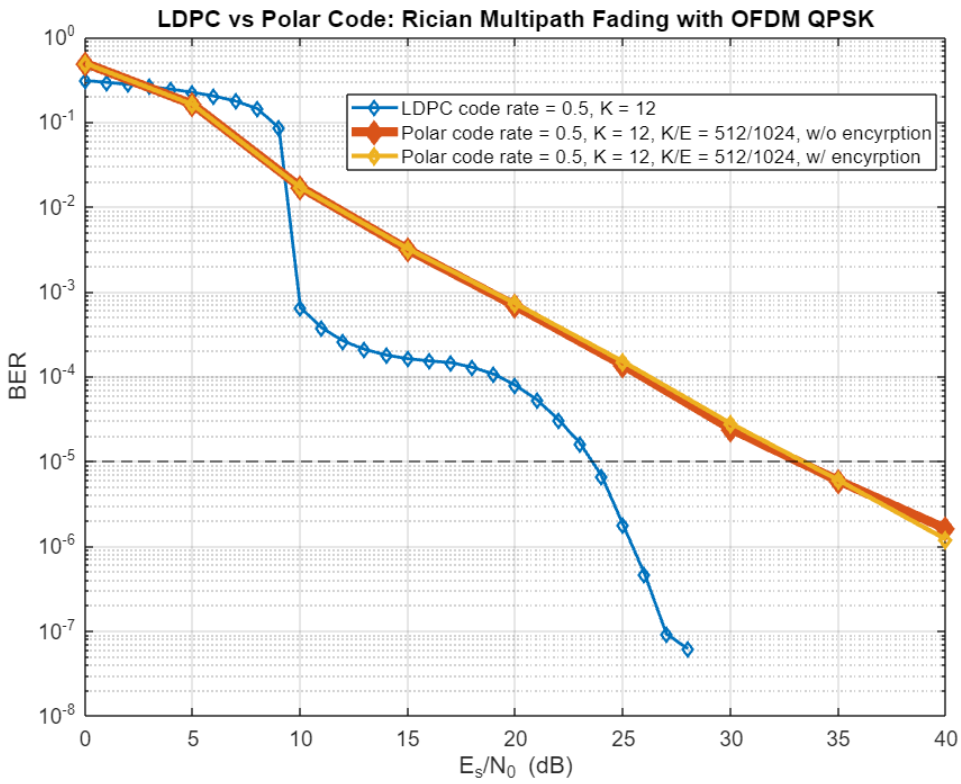


**Figure 36. BER versus SNR Under Two Multipath Rician Fading with Rician Factor *K*= 12 dB**

# 5 CONCLUSIONS

Models and simulations were developed to compare the performance for an additive white Gaussian noise (AWGN) channel, a Rayleigh fading channel, and a Rician fading channel. Both flat and frequency selective channels were considered for the later two models. Simulations were performed using channel attenuation data measured at 72 GHz from the W/V-band Terrestrial Link Experiment. Analysis was presented using the DVB-S2 protocol. Results suggest that multipath fading significantly deteriorates performance.

Models and simulations were developed that implemented orthogonal frequency division multiplexing (OFDM), similar to that used by 5G wireless commercial networks. Implementation of OFDM improved performance against severe multipath fading environments. However, the bit error rate performance was worse than under a no-fading, AWGN channel.

Models and simulations were developed to investigate polar forward error-correction code (FEC) as a replacement for the LDPC coding used by DVB-S2. Different fading models were applied. Results suggest performance is strongly dependent on the actual channel fading conditions.

Models and simulations were developed to investigate the performance impacts of double-layer encryption. The 5G polar code and DVB-S2 LDPC code were used as forward error correction codes in the investigation. Different fading models were applied. Results suggest performance is strongly dependent on the actual channel fading conditions. However, even short encryption key were very successful at thwarting eavesdropping on wireless communications. Further, the same performance was observed regardless of key length. This implies that the additional complexity to employ the encryption and decryption is negligible. Finally, the additional delay caused by encryption and decryption for the 5G network is also negligible because only modulo-2 addition is required.

## REFERENCES


[1] E. S. Hong, S. Lane, D. Murrell, N. Tarasenko, C. Christodoulou, and J. Keeley, "Estimating Rain Attenuation at 72 and 84 GHz from Raindrop Size Distribution Measurements in Albuquerque, NM, USA," *IEEE Geo-science and Remote Sensing Letters*, pp. 1175-1179, 2019.

[2] N. Tarasenko, S. Lane, D. Murrell, N. Tarasenko, C. Christodoulou, J. Nessel, M. Zemba, and J. Houts, "W/V-band Terrestrial Link Experiment, An Overview," *IEEE International Symposium on Antennas and Propagation*, pp. 1259-1260, 2016.

[3] Hyuck M. Kwon, Richard Lahman, and Ian Ellis Hulede, *Future W/V-Band Satellite Communication Systems*, AFRL-RV-PS-TR-2021-0100, Wichita State University, Wichita, KS, September 20, 2021.

[4] Richard Lahman, Ian Ellis Hulede, Hyuck M. Kwon, David Murrell, and Steven Lane, "Conversion from Channel Attenuation to Data Rate Estimation," *2021 IEEE Aerospace Conference*, Yellowstone Conference Center, Big Sky, Montana, pp. 1-6, Mar 6-13, 2021.

[5] ETSI, "Digital Video Broadcasting (DVB); Second Generation Framing Structure, Channel Coding and Modulation Systems for Broadcasting, Interactive Services, New Gathering and Other Broadband Satellite Applications," EN 302 307-1 v1.2.1 (2009-04).

[6] R. Gallager, "Low-Density Parity-Check Codes," *IRE Transactions on Information Theory*, pp. 21-28, 1962.

[7] D. MacKay, "Good Error-Correcting Codes Based On Very Sparse Matrices," *IEEE Transactions on Information Theory*, pp. 399-431, 1999.

[8] *3GPP, in 3rd Generation Partnership Project*, Technical Specification Group Radio Access Network, Physical Channels and Modulation (Release 17), 3GPP TS 38.211 v17.0.0, December 2021.

[9] 3GPP, in 3rd Generation Partnership Project, Technical Specification Group Radio Access Network, Physical Layer Procedures for Control (Release 17), 3GPP TS 38.213 v17.0.0, December 2021.

[10] 3GPP, in 3rd Generation Partnership Project, Technical Specification Group Radio Access Network, Physical Layer Measurements (Release 17), 3GPP TS 38.215 v17.0.0, December 2021.

[11] Richard Lahman and Hyuck M. Kwon, "Low Density Parity Check Code in DVB-S2 Verses Polar Code under SATCOM Fading," *2023 IEEE Aerospace Conference*, Yellowstone, Big Sky, MT, March 4-11, 2023.

[12] T. Pratt and J. Allnutt, *Satellite Communications*, 3rd edition, "DVB-S and DVB-S2 Standards," John Wiley and Sons, Hoboken, NY, 2023, pp. 556-568.

[13] B. P. Lathi and Z. Ding, *Modern Digital and Analog Communication Systems*, 4th edition, "Principles of Digital Data Transmission," Oxford University Press, New York, 2009, pp. 377-446.

[14] R. E. Ziemer and W. H. Tranter, *Principles of Communications, Systems Modulation and Noise*, 6th edition, "Multipath Interference," John Wiley and Sons, Hoboken, NJ, 2009, pp. 431-437.

[15] R. E. Ziemer and W. H. Tranter, *Principles of Communications, Systems Modulation and Noise*, 6th edition, "Flat Fading Channels," John Wiley and Sons, Hoboken, NJ, 2009, pp. 437-441.

[16] Erdal Arikan, "Channel Polarization: A Method for Constructing Capacity-Achieving Codes for Symmetric Binary-Input Memoryless Channels," *IEEE Transactions on Information Theory*, Vol. 55, No. 7, pp. 3051-3073, July 2009.

## APPENDIX 1 MATLAB Source Code for Flat Rayleigh Fading

```
%****** Es/No to Eb/No conversion ******
(line 1) EbNodB = EsNodB-10*log(log2(dvb.ModulationOrder));
(line 2) EbNo = 10^(EbNodB/10);
%*************************************

%***** Modulation block ***********
(line 3) if dvb.ModulationOrder == 4 || dvb.ModulationOrder == 8
                modOut = pskModulator(intrlvrOut);
(line 4) else
(line 5)                        modOut = dvbsapskmod(intrlvrOut, dvb.ModulationOrder, 's2', ...
                dvb.CodeRate, 'InputType', 'bit', 'UnitAveragePower', true);
(line 6) end
%*********************************

%***** Rayleigh Fading channel **************
(line 7) h_c = sqrt(1/2).*randn(1,length(modOut));
(line 8) h_s = sqrt(1/2).*randn(1,length(modOut));
(line 9) h = h_c + sqrt(-1).*h_s;
(line 10) noise =(1/sqrt(2*EbNo))*(randn(1,length(modOut))...
        +1i*randn(1,length(modOut)));  %Random noise generation
        noise = noise./h;
(line 11) chanOut2 = modOut + transpose(noise);
%*****************************************

%***** Demodulation block **********
(line 12) if dvb.ModulationOrder == 4 || dvb.ModulationOrder == 8
(line 13)         demodOut = pskDemodulator(chanOut2);
(line 14) else
(line 15)         demodOut = dvbsapskdemod(chanOut2, dvb.ModulationOrder, 's2', ...
                dvb.CodeRate, 'OutputType', 'approxllr', 'NoiseVar', ...
                dvb.NoiseVar, 'UnitAveragePower', true);
(line 16) end
%*********************************
```

## APPENDIX 2 MATLAB Source Code for Frequency Selective Rayleigh Fading

```
%******Rayleigh Fading Multipath OFDM parameters
(line 1) Ns = 1024;
(line 2) h_n = zeros(1, Ns);
(line 3) var0 = 0.7;
(line 4) var1 = 0.3;
(line 5) sd0 = sqrt(var0);
(line 6) sd1 = sqrt(var1);
(line 7) ccc = ceil(dvb.NumSymsPerCodeword/Ns);
(line 8) vv = ccc*Ns-dvb.NumSymsPerCodeword;
(line 9) zz = zeros(vv,1);
%************************************

%******Es/No to Eb/No conversion ******
(line 10) EbNodB = EsNodB-10*log(log2(dvb.ModulationOrder));
(line 11) EbNo = 10^(EbNodB/10);
%************************************

%***** Modulation block ***********
(line 12) if dvb.ModulationOrder == 4 || dvb.ModulationOrder == 8
        modOut = pskModulator(intrlvrOut);
(line 13) else
(line 14)         modOut = dvbsapskmod(intrlvrOut, dvb.ModulationOrder, 's2', ...
                  dvb.CodeRate, 'InputType', 'bit', 'UnitAveragePower', true);
(line 15) end
%**********************************

%***** Rayleigh Multipath Fading channel with OFDM **************
(line 16) modOut_Q = [modOut;zz];
(line 17) ser_2_par = reshape(modOut_Q,[1024,ccc]);
(line 18) h0 = (sd0/sqrt(2))*(randn + 1j*randn);
(line 19) h1 = (sd1/sqrt(2))*(randn + 1j*randn);
(line 20) h_n(1) = h0;
(line 21) h_n(4) = h1;
(line 22) H = fft(h_n)';     % create H matrix using FFT of h_n

(line 23) for t = 1:ccc
(line 24)         r_k(:,t) = chan(H.*ser_2_par(:,t));
(line 25)         s_hat(:,t) = r_k(:,t)./H;
(line 26) end

(line 27) par_2_ser = reshape(s_hat,[ (dvb.NumSymsPerCodeword+vv),1]);
(line 28) chanOut2 = par_2_ser(1:end-vv,:);
```

```
%*****************************************

%***** Demodulation block **********
(line 29) if dvb.ModulationOrder == 4 || dvb.ModulationOrder == 8
(line 30)         demodOut = pskDemodulator(chanOut2);
(line 31) else
(line 32)         demodOut = dvbsapskdemod(chanOut2, dvb.ModulationOrder, 's2', ...
                  dvb.CodeRate, 'OutputType', 'approxllr', 'NoiseVar', ...
                  dvb.NoiseVar, 'UnitAveragePower', true);
(line 33) end
%*************************************
```

## APPENDIX 3 MATLAB Source Code for Flat Rician Fading

```
%******Rician Fading Parameters ******
(line 1) Pr_av=1;  %Average receive power
(line 2) K = 12;    %Rician Factor K
(line 3) mu = sqrt(K*Pr_av/((K+1)));     %Square root of power in LOS component
(line 4) sigma =sqrt(Pr_av/(2*(K+1)));  %Square root of power in the non-LOS component
%*************************************

%******Es/No to Eb/No conversion ******
(line 5) EbNodB = EsNodB-10*log(log2(dvb.ModulationOrder));
(line 6) EbNo = 10^(EbNodB/10);
%*************************************

%***** Modulation block ***********
(line 7) if dvb.ModulationOrder == 4 || dvb.ModulationOrder == 8
                modOut = pskModulator(intrlvrOut);
(line 8) else
(line 9)                        modOut = dvbsapskmod(intrlvrOut, dvb.ModulationOrder, 's2', …
                dvb.CodeRate, 'InputType', 'bit', 'UnitAveragePower', true);
(line 10) end
%*********************************

%***** Rayleigh Fading channel **************
(line 11) h_coef = ((sigma*randn(1,length(modOut))+mu)
                +1i*(sigma*randn(1,length(modOut))+mu));
(line 12) noise = (1/sqrt(2*EbNo))*(randn(1,length(modOut))+1i*randn(1,length(modOut)));
(line 13) noiseRician = transpose(noise./h_coef);
(line 14) chanOut2 = modOut + noiseRician;
%*****************************************

%***** Demodulation block **********
(line 15) if dvb.ModulationOrder == 4 || dvb.ModulationOrder == 8
(line 16)         demodOut = pskDemodulator(chanOut2);
(line 17) else
(line 18)         demodOut = dvbsapskdemod(chanOut2, dvb.ModulationOrder, 's2', ...
                dvb.CodeRate, 'OutputType', 'approxllr', 'NoiseVar', ...
                dvb.NoiseVar, 'UnitAveragePower', true);
(line 19) end
%*********************************
```

## APPENDIX 4 MATLAB Source Code for Frequency Selective Rician Fading

```
%******Rician parameters
(line 1) K_dB=12;
(line 2) Pr_av=1;
(line 3) K = 10.^(K_dB/10);
(line 4) mu=sqrt(K*Pr_av/((K+1)));
(line 5) sigma=sqrt(Pr_av/(2*(K+1)));
%************************************

(line 6) Ns = 1024;
(line 7) bPoint = 1;
(line 8) ePoint = Ns;
(line 9) r_k = [];
(line 10) chanOut2 = [];

%******Es/No to Eb/No conversion ******
(line 11) EbNodB = EsNodB-10*log(log2(dvb.ModulationOrder));
(line 12) EbNo = 10^(EbNodB/10);
%************************************

%***** Modulation block ***********
(line 13) if dvb.ModulationOrder == 4 || dvb.ModulationOrder == 8
                modOut = pskModulator(intrlvrOut);
(line 14) else
(line 15)       modOut = dvbsapskmod(intrlvrOut, dvb.ModulationOrder, 's2', ...
                dvb.CodeRate, 'InputType', 'bit', 'UnitAveragePower', true);
(line 16) end
%*********************************

%***** Rician Multipath Fading channel with OFDM **************
(line 17) modOut_Q = [modOut;zz];
(line 18) for tt = 1:ccc
(line 19)       if tt == ccc
(line 20)               subCarrier_block = modOut(bPoint:end,1);
(line 21)               h_n = zeros(1, length(subCarrier_block));
(line 22)       else
(line 23)               subCarrier_block = modOut(bPoint:ePoint,1);
(line 24)               h_n = zeros(1, Ns);
(line 25)       end
(line 26)       h_coef_0=sqrt(0.7)*((sigma*randn+mu)+1i*(sigma*randn+mu))./sqrt(2);
(line 27)       h_coef_0=sqrt(0.3)*((sigma*randn+mu)+1i*(sigma*randn+mu))./sqrt(2);
(line 28)       h_n(1) = h_coef_0;
(line 29)       h_n(4) = h_coef_1;
```

```
(line 30)       H = fft(h_n); % create H matrix using FFT of h_n
(line 31)       r_k = chan(H'.*subCarrier_block);
(line 32)       s_hat = r_k./H';
(line 33)       chanOut2 = [chanOut2 ;s_hat];
(line 34)
(line 35)       bPoint = ePoint+1;
(line 36)       ePoint = ePoint + Ns;
(line 37)       subCarrier_block = [];
(line 38) end
%*****************************************

%***** Demodulation block **********
(line 39) if dvb.ModulationOrder == 4 || dvb.ModulationOrder == 8
(line 40)       demodOut = pskDemodulator(chanOut2);
(line 41) else
(line 42)       demodOut = dvbsapskdemod(chanOut2, dvb.ModulationOrder, 's2', ...
                dvb.CodeRate, 'OutputType', 'approxllr', 'NoiseVar', ...
                dvb.NoiseVar, 'UnitAveragePower', true);
(line 43) end
%************************************
```

## APPENDIX 5 MATLAB Source Code for 5G Polar FEC and Flat Rayleigh Fading

```
(line 1) s = rng(100);  % Seed the RNG for repeatability

% ********** Code parameters **********
(line 2) K = 54;       % Message length in bits, including CRC, K > 30
(line 3) E = 124;      % Rate matched output length, E <= 8192
%************************************

% ********** Rayleigh Fading multipath parameters **********
(line 4) var0 = 0.7;
(line 5) var1 = 0.3;
(line 6) sd0 = sqrt(var0);
(line 7) sd1 = sqrt(var1);
(line 8) EbNo_range = 0:1:35;   % Eb/No in dB
(line 9) rangeLength = length(EbNo_range);
(line 10) blockErrorRate = zeros(rangeLength);
(line 11) polar_BER = zeros(rangeLength,1);
(line 12) SNR_dB = zeros(rangeLength,1);
%************************************

(line 13) for y=1:length(EbNo_range)
(line 14)         EbNo = EbNo_range(y);
(line 15)         L = 8;                    % List length, a power of two, [1 2 4 8]
(line 16)         numFrames = 30000;    % Number of frames to simulate
(line 17)         linkDir = 'DL';           %Link direction: downlink('DL') OR uplink ('UL')

(line 18)         if strcmpi(linkDir,'DL')   % Downlink scenario (K >= 36, including CRC bits)
(line 19)                 crcLen = 24;      % Number of CRC bits for DL, Section 5.1, [6]
(line 20)                 poly = '24C';     % CRC polynomial
(line 21)                 nPC = 0;          % Number of parity check bits, Section 5.3.1.2, [6]
(line 22)                 nMax = 9;         % Maximum value of n, for 2^n, Section 7.3.3, [6]
(line 23)                 iIL = true;       % Interleave input, Section 5.3.1.1, [6]
(line 24)                 iBIL = false;     % Interleave coded bits, Section 5.4.1.3, [6]
(line 25)         else                      % Uplink scenario (K > 30, including CRC bits)
(line 26)                 crcLen = 11;
(line 27)                 poly = '11';
(line 28)                 nPC = 0;
(line 29)                 nMax = 10;
(line 30)                 iIL = false;
(line 31)                 iBIL = true;
(line 32)         end

(line 33)         R = K/E;                % Effective code rate
```

```
(line 34)       bps = 2;                % bits per symbol, 1 for BPSK, 2 for QPSK
(line 35)       EsNo = EbNo + 10*log10(bps);
(line 36)       snrdB = EsNo + 10*log10(R);       % in dB
(line 37)       noiseVar = 1./(10.^(snrdB/10));

                % Channel
(line 38)       chan=comm.AWGNChannel('NoiseMethod','Variance','Variance',noiseVar);
(line 39)       ber = comm.ErrorRate;
(line 40)       numferr = 0;

(line 41)       for i = 1:numFrames
(line 42)           % Generate a random message
(line 43)           msg = randi([0 1],K-crcLen,1);

(line 44)           % Attach CRC
(line 45)           msgcrc = nrCRCEncode(msg,poly);

(line 46)           % Polar encode
(line 47)           encOut = nrPolarEncode(msgcrc,E,nMax,iIL);
(line 48)           N = length(encOut);

(line 49)           % Rate match
(line 50)           modIn = nrRateMatchPolar(encOut,K,E,iBIL);

(line 51)           % Modulate
(line 52)           modOut = nrSymbolModulate(modIn,'QPSK');

(line 53)           % ----Add White Gaussian noise only----
(line 54)           %  rSig = chan(modOut);

                    % Rayleigh Fading Single path case-------
                    % Rayleigh channel
(line 55)           h = 1/sqrt(2)*(randn(length(modOut),1) + 1i*randn(length(modOut),1));
(line 56)           h_abs = abs(h);
(line 57)           yy = chan(h_abs.*modOut);
(line 58)           rSig = (yy./h_abs);
(line 59)           %-------------------------------------------------

(line 60)           % Rayleigh Fading Multipath with OFDM case----------
(line 61)           % h_n = zeros(1, length(modOut));
(line 62)           % modOut_Q = modOut;
(line 63)           % h0 = (sd0/sqrt(2))*(randn + 1j*randn);
(line 64)           % h1 = (sd1/sqrt(2))*(randn + 1j*randn);
```

```
(line 65)                % h_n(1) = h0;
(line 66)                % h_n(4) = h1;
(line 67)                % H = fft(h_n)'; % create H matrix using FFT of h_n
(line 68)                %
(line 69)                % r_k = chan(H.*modOut_Q);
(line 70)                % s_hat = r_k./H;
(line 71)                % rSig = s_hat;
(line 72)                %---------------------------------------

(line 73)                % Soft demodulate
(line 74)                rxLLR = nrSymbolDemodulate(rSig,'QPSK',noiseVar);

(line 75)                % Rate recover
(line 76)                decIn = nrRateRecoverPolar(rxLLR,K,N,iBIL);

(line 77)                % Polar decode
(line 78)                decBits = nrPolarDecode(decIn,K,E,L,nMax,iIL,crcLen);

(line 79)                % Compare msg and decoded bits
(line 80)                errStats = ber(double(decBits(1:K-crcLen)), msg);
(line 81)                numferr = numferr + any(decBits(1:K-crcLen)~=msg);

(line 82)        end

(line 83)        disp(['Simulated at : ' num2str(EbNo) ' dB'])
(line 84)        disp(['Block Error Rate: ' num2str(numferr/numFrames) ...
(line 85)        ', Bit Error Rate: ' num2str(errStats(1)) ...
(line 86)        ', at SNR = ' num2str(snrdB) ' dB'])
(line 87)        blockErrorRate(y) = numferr/numFrames;
(line 88)        polar_BER(y) = errStats(1);
(line 89)        SNR_dB(y) = snrdB;

(line 90)        rng(s);   % Restore RNG
(line 91) end
```

## APPENDIX 6 MATLAB Source Code for Double Layer Encryption

```
s = rng(100);      % Seed the RNG for repeatability

% Code parameters
K = 512;           % Message length in bits, including CRC, K > 30
E = 1024;          % Rate matched output length, E <= 8192

% Rayleigh Fading multipath parameters
% Ns = K;
% %h_n = zeros(1, Ns);
% var0 = 0.7;
% var1 = 0.3;
% sd0 = sqrt(var0);
% sd1 = sqrt(var1);

% Rician fading parameters
K_dB=12;
Pr_av=1;
K_rician = 10.^(K_dB/10);
mu=sqrt(K_rician*Pr_av/((K_rician+1)));
sigma=sqrt(Pr_av/(2*(K_rician+1)));

% encryption key
key_Alice = randi([0,1],K-11,1);        %uplink case
key_Eve = randi([0,1],K-11,1);          %uplink case

% short_key = randi([0,1],1,4);                          %short key
% key_Alice = [(repmat(short_key,1,125))'; 0];           %short key

% EbNo = 1;        % EbNo in dB
EbNo_range = 0:5:40;                % Eb/No in dB
rangeLength = length(EbNo_range);
blockErrorRate = zeros(rangeLength);
polar_BER = zeros(rangeLength,1);
SNR_dB = zeros(rangeLength,1);

for y=1:length(EbNo_range)
    EbNo = EbNo_range(y);
    L = 8;                      % List length, a power of two, [1 2 4 8]
    numFrames = 40000;          % Number of frames to simulate
    linkDir ='UL';              % Link direction: downlink ('DL') OR uplink ('UL')

    % Specify the code parameters used for a simulation
```

```
if strcmpi(linkDir,'DL')
        % Downlink scenario (K >= 36, including CRC bits)
        crcLen = 24;    % Number of CRC bits for DL, Section 5.1, [6]
        poly = '24C';   % CRC polynomial
        nPC = 0;        % Number of parity check bits, Section 5.3.1.2, [6]
        nMax = 9;       % Maximum value of n, for 2^n, Section 7.3.3, [6]
        iIL = true;     % Interleave input, Section 5.3.1.1, [6]
        iBIL = false;   % Interleave coded bits, Section 5.4.1.3, [6]
else
        % Uplink scenario (K > 30, including CRC bits)
        crcLen = 11;
        poly = '11';
        nPC = 0;
        nMax = 10;
        iIL = false;
        iBIL = true;
end

R = K/E;                % Effective code rate
bps = 2;                % bits per symbol, 1 for BPSK, 2 for QPSK
EsNo = EbNo + 10*log10(bps);
snrdB = EsNo + 10*log10(R);         % in dB
noiseVar = 1./(10.^(snrdB/10));

% Channel
chan = comm.AWGNChannel('NoiseMethod','Variance','Variance',noiseVar);

ber = comm.ErrorRate;

numferr = 0;

for i = 1:numFrames

        % Generate a random message
        msg = randi([0 1],K-crcLen,1);

        % encryption the message here
        msgEncrypt = mod(msg+key_Alice,2);

        % Attach CRC with encyrption
        msgcrc = nrCRCEncode(msgEncrypt,poly);
```

```
% Attach CRC without encryption
%msgcrc = nrCRCEncode(msg,poly);

% Polar encode
encOut = nrPolarEncode(msgcrc,E,nMax,iIL);
N = length(encOut);

% Rate match
modIn = nrRateMatchPolar(encOut,K,E,iBIL);

% Modulate
modOut = nrSymbolModulate(modIn,'QPSK');

% Add White Gaussian noise
%rSig = chan(modOut);

% Rayleigh Fading Single path case-----------------------------
% h_c = sqrt(1/2).*randn(1,length(modOut));
% h_s = sqrt(1/2).*randn(1,length(modOut));
% h = (h_c + sqrt(-1).*h_s)';

% Random noise generation
% noise =((sqrt(noiseVar)/sqrt(2))* ...
          (randn(1,length(modOut))+1i*randn(1,length(modOut))))';
% noise = noise./h;
% rSig = modOut + noise;

% Rayleigh channel
% h = 1/sqrt(2)*(randn(length(modOut),1) + 1i*randn(length(modOut),1));

% h_abs = abs(h);
% yy = chan(h_abs.*modOut);
% rSig = (yy./h_abs);
%-----------------------------------------------

% Rayleigh Fading Multipath case with OFDM----------
% h_n = zeros(1, length(modOut));
% modOut_Q = modOut;
% h0 = (sd0/sqrt(2))*(randn + 1j*randn);
% h1 = (sd1/sqrt(2))*(randn + 1j*randn);
% h_n(1) = h0;
% h_n(4) = h1;
% H = fft(h_n)';                    % create H matrix using FFT of h_n
```

```
            %
            % r_k = chan(H.*modOut_Q);
            % s_hat = r_k./H;
            % rSig = s_hat;
            %---------------------------------------

            % new Rician Multipath fading w/ OFDM ------------------
            h_n = zeros(1, length(modOut));
            modOut_Q = modOut;
            h_coef_0=((sigma*randn+mu)+1i*(sigma*randn+mu))./sqrt(2);
            h_coef_1=((sigma*randn+mu)+1i*(sigma*randn+mu))./sqrt(2);
            h_n(1) = sd0.*h_coef_0;
            h_n(4) = sd1.*h_coef_1;
            H = fft(h_n)';                  % create H matrix using FFT of h_n
            r_k = chan(H.*modOut_Q);
            rSig = r_k./H;

            % Soft demodulate
            rxLLR = nrSymbolDemodulate(rSig,'QPSK',noiseVar);

            % Rate recover
            decIn = nrRateRecoverPolar(rxLLR,K,N,iBIL);

            % Polar decode without encryption
            %decBits = nrPolarDecode(decIn,K,E,L,nMax,iIL,crcLen);

            % Polar decode with encryption
            decBits = nrPolarDecode(decIn,K,E,L,nMax,iIL,crcLen);

            % Decrypt the message here with encryption
            msgDecrypt = mod((decBits(1:K-crcLen))+key_Alice,2);

            % Compare msg and decoded bits encrypted
            errStats = ber(double(msgDecrypt), msg);
            numferr = numferr + any(msgDecrypt~=msg);

            % Compare msg and decoded bits
            %errStats = ber(double(decBits(1:K-crcLen)), msg);
            %numferr = numferr + any(decBits(1:K-crcLen)~=msg);
end

disp(['Simulated at : 'num2str(EbNo)' dB'])
disp(['Block Error Rate: 'num2str(numferr/numFrames)...
```

```
                , Bit Error Rate: 'num2str(errStats(1))...
                , at SNR = 'num2str(snrdB)' dB'])
        blockErrorRate(y) = numferr/numFrames;
        polar_BER(y) = errStats(1);
        SNR_dB(y) = snrdB;
end
```

## LIST OF SYMBOLS, ABBREVIATIONS AND ACRONYMS

| | |
|---|---|
| 3GPP | Third Generation Partnership Project |
| 4G | Fourth Generation |
| 4QAM | Four Quadrature Amplitude Multitude |
| 5G | Fifth Generation |
| 6G | Sixth Generation |
| 8PSK | 8 Phase Shift Keying |
| 16APSK | 16 Amplitude Phase Shift Keying |
| 16QAM | 16 Quadrature Amplitude Modulation |
| 32APSK | 32 Amplitude Phase Shift Keying |
| 64QAM | 64 Quadrature Amplitude Modulation |
| ACM | Adaptive Code Modulation |
| AWGN | Additive White Gaussian Noise |
| BCH | Bose-Chaudhuri-Hocquenghem |
| BER | Bit Error Rate |
| BS | Base Station |
| BW | Bandwidth |
| BWE | Bandwidth Efficiency |
| CDF | Cumulative Distribution Function |
| CFR | Channel Frequency Response |
| CIR | Channel Impulse Response |
| dB | Decibel (relative to 1 Watt) |
| dBm | Decibel (relative to 1 milli-Watt) |
| DL | Downlink |
| DVB-S2 | Digital Video Broadcasting - Second Generation |
| Es | Symbol Energy |
| FEC | Forward Error Correction |
| FFT | Fast Fourier Transform |
| Gbps | Giga Bits Per Second |

| | |
|---|---|
| GHz | Giga Hertz |
| Hz | Hertz (cycles per second) |
| IC | Integrated Circuits |
| IFFT | Inverse Fast Fourier Transform |
| LDPC | Low Density Parity Check |
| LOS | Line of Sight |
| M | Number of Constellation Points |
| MRC | Maximum Ratio Combining |
| NASA | National Aeronautical and Space Administration |
| NLOS | Non Line of Sight |
| No | Noise Power |
| NTN | Non-Territorial Network |
| OFDM | Orthogonal Frequency Division Multiplexing |
| PER | Packet Error Rate |
| PI | Principal Investigator |
| PMF | Probability Mass Function |
| PTW | Protected Tactical Waveform |
| QPSK | Quadrature Phase Shift Keying |
| Rc | Code Rate |
| RF | Radio Frequency |
| RX | Receiver |
| SIM | Subscriber Identity Module |
| SNR | Signal to Noise Ratio |
| TN | Terrestrial Network |
| Ts | Sample Period |
| TX | Transmitter |
| UE | User Equipment |
| UTC | Universal Coordinated Time |

## DISTRIBUTION LIST

DTIC/OCP
8725 John J. Kingman Rd, Suite 0944
Ft Belvoir, VA 22060-6218 1 cy

AFRL/RVIL
Kirtland AFB, NM 87117-5776 1 cy

Official Record Copy
AFRL/RVB/Dr. Steven A. Lane 1 cy